Stress testing insurance market stability under climate risk

Simona Meiler[1,*], Steven I. Jackson[2], Kerry Emanuel[3], Noah S. Diffenbaugh[4], and Jack W. Baker[1]

[1]Civil and Environmental Engineering, Stanford University, CA, USA
[2]American Academy of Actuaries, Washington, DC, USA
[3]Lorenz Center, Massachusetts Institute of Technology, Cambridge, Massachusetts, USA
[4]Earth System Science, Stanford University, CA, USA
[*]Corresponding author: simona@simonameiler.ch

This manuscript is a non–peer-reviewed preprint submitted to EarthArXiv and currently under review. The content has not yet been certified by peer review and may be subject to change.

ABSTRACT

Climate change, urban development, and evolving insurance markets threaten the stability of disaster-risk financing. Homeowners insurance is embedded in a layered network of reinsurers, capital markets, and public backstops that can be overwhelmed by extreme events. We develop a probabilistic risk propagation model linking tropical cyclone wind and flood losses to Florida's residential insurance market, backstops, and regulatory thresholds. Between 10- and 100-year tropical cyclone seasons, total losses increase ninefold while public burden increases more than fortyfold as institutional thresholds and capital constraints bind. We estimate a 3.7% annual probability that hurricane-related public burden exceeds 1% of Florida's GDP, a fiscal scale comparable to public costs of systemic banking crises. By evaluating climate change, market dynamics, and adaptation within the same quantitative framework, we provide a transferable template for stress-testing insurance systems and identifying whether policy and market changes reduce losses or shift burdens across households, insurers, and public institutions.

Introduction

The 2017 Atlantic hurricane season, including Hurricanes Harvey, Irma, and Maria, caused more than USD 260 billion in economic losses (unadjusted for inflation) (1), making 2017 the costliest year on record for insured catastrophe losses at the time (2). The increasing likelihood of many weather and climate extremes (3) and of compound events (4) erodes the stationarity that underpins traditional disaster risk assessment and pricing (5). Disaster insurance transfers losses from households to insurers and state-backed providers, allowing post-disaster repair, supporting mortgage markets, and accelerating economic recovery after extreme events (5, 6). Primary insurers absorb losses up to their capital and reinsurance protection, after which risks propagate to reinsurers, catastrophe bond investors, and public backstops such as state insurance programs or federal institutions. Under moderate shocks, this structure spreads risk efficiently; under extreme or clustered events, however, contractual limits, capital constraints, and regulatory thresholds can bind, causing losses to cascade across institutions rather than being smoothly absorbed (7–9). A single costly year is within the volatility that capital and reinsurance are designed to absorb. Less certain is whether intensifying hazards and growing insurance market strain push an increasing share of losses beyond the system's capacity and onto households and the public (10, 11).

In California, constraints on rate-making and the prohibition on forward-looking catastrophe models, together with rising wildfire losses, have driven a wave of insurer withdrawals (12–14). In Florida, repeated tropical cyclone (TC) losses have produced insurer insolvencies, rapid premium increases, and growing reliance on the residual market (15–17). In both states, risk increasingly shifts back to households and public institutions beyond the scale for which these mechanisms were designed, raising concerns that climate-driven disasters may transition from diversifiable shocks to systemic insurance market stress. These dynamics also matter because insurance prices and availability can communicate underlying risk, whereas subsidized or publicly backstopped coverage that preserves affordability without reducing exposure can weaken incentives for mitigation and continued development in high-risk areas (18–21).

Despite growing recognition that climate-driven disasters pose systemic financial risks, insurance markets lack quantitative system-wide stress tests of the kind used to assess stability in banking. In the banking sector, stress testing is a central tool for evaluating the resilience of complex financial systems to rare but severe shocks, focusing on tail risks and the potential for

cascading failures (22–24). Climate-related financial-risk exercises have begun to extend this stress testing logic, building on academic proposals for climate stress testing (25) and coordinated through the Network for Greening the Financial System (26). To date, these climate applications have remained largely exploratory: the European Central Bank's economy-wide and supervisory climate stress tests (27, 28) and the Bank of England's 2021 Climate Biennial Exploratory Scenario (29) carried no direct capital implications, and the U.S. Federal Reserve's 2023 exercise was a voluntary pilot with no capital or supervisory implications (30). By contrast, climate risk assessments in insurance have largely centered on catastrophe loss reporting, disclosure frameworks, and firm-level solvency exercises (31–35), which are not designed to quantify when aggregate losses overwhelm market-wide capacity, trigger public backstops, or propagate across interconnected private and public actors. This gap is increasingly consequential as climate change shifts the frequency and clustering of extreme events.

Here, we develop a probabilistic, system-wide stress testing framework that links physical hazard, market structure, and public backstops to quantify systemic insurance stress and the resulting public burden. The framework propagates physics-based simulations of TC wind and flood losses through the full layered architecture of primary insurers, reinsurance and capital markets, the residual market, the guaranty fund, and state and federal backstops, tracking at each step how much loss is absorbed, where contractual limits and statutory thresholds bind, and how much residual loss falls on households and public institutions (Fig. 1). We apply it to the Florida residential property insurance market, where high exposure to TCs, dense coastal development (36), and recent insurer insolvencies following Hurricane Ian (15) make systemic risk an immediate concern (9). We simulate losses from historical TCs (37), stylized sequential events, and large probabilistic event sets representing present-day and future climate conditions (38, 39), and evaluate the system under stylized market and policy scenarios. With this framework, we ask when and where climate-driven losses overwhelm the system and accumulate as a public burden, and how climate change, market structure, and adaptation reshape that risk.

Florida is an early manifestation of climate-related insurance stress (9). While institutional details vary across regions and hazards, layered risk transfer is a common feature of disaster insurance systems. Our framework provides a transferable approach for identifying where extreme losses accumulate, under which conditions private capacity is overwhelmed, and how policy interventions reshape systemic risk.

Insurance system architecture and risk propagation

We first summarize the structure of the Florida residential insurance system and the pathways through which TC losses propagate across private insurers, reinsurers, capital markets, and public backstops (Fig. 1c).

In the first layer of risk absorption, losses are distributed between four primary holders of risk: private admitted-market insurers providing wind coverage, Citizens Property Insurance Corporation as Florida's residual wind insurer (40), the U.S. National Flood Insurance Program (NFIP) providing flood coverage (41), and households that are uninsured or underinsured. Uninsured and underinsured losses arise both voluntarily, through coverage choices and deductibles, and involuntarily, due to limited insurance availability or policy caps. The NFIP is a federally administered program that offers standardized flood insurance nationwide, while private insurers and Citizens operate at the state level and primarily cover wind-related losses. For each of these entities, we compile exposure data (total insured value and coverage-in-force), which determine how gross TC damages are initially allocated.

In a second layer, we represent formal risk transfer mechanisms that redistribute insured losses. Private insurers and Citizens purchase reinsurance through the Florida Hurricane Catastrophe Fund (FHCF), a state-run public reinsurance program with company-specific retentions and a statewide seasonal payout cap (42, 43). Some insurers and Citizens additionally transfer risk to capital markets via catastrophe bonds (44). The NFIP, by contrast, does not rely on reinsurance; flood claims are paid from the national NFIP pool and, when that pool is insufficient, through borrowing from the U.S. Treasury (45). At this stage, insured losses are transformed into net losses for each primary insurer after accounting for reinsurance recoveries, cat bond payouts, and regulatory caps.

A final layer captures institutional backstops and loss-sharing mechanisms that activate when insurer capital is insufficient. Insolvent private insurers trigger assessments through the Florida Insurance Guaranty Association (FIGA), which levies assessments on surviving insurers, subject to statutory caps, to cover policyholder claims (46, 47). Citizens operates under a separate, tiered assessment framework: Tier 1 assessments are levied on Citizens' own policyholders, while Tier 2 assessments can be applied to nearly all property insurance policies statewide, up to prescribed limits (48). The NFIP has no analogous constraint; losses exceeding the NFIP fund balance are recorded as federal borrowing, effectively transferring flood losses to the national public balance sheet (45).

We formulate our quantitative systemic risk assessment around this insurance system architecture, evaluating single and sequential historical TCs as well as probabilistic event sets representing present and future climate conditions (Fig. 1b). Across

all simulations, we track the initial loss decomposition across households and insurance entities, the redistribution of losses after risk transfer, insurer capital depletion and defaults, activation of public backstops, and a set of system-level metrics that quantify institutional stress and public burden (Fig. 1d). Full details of data sources, regulatory parameters, and implementation are provided in Section Insurance market data.

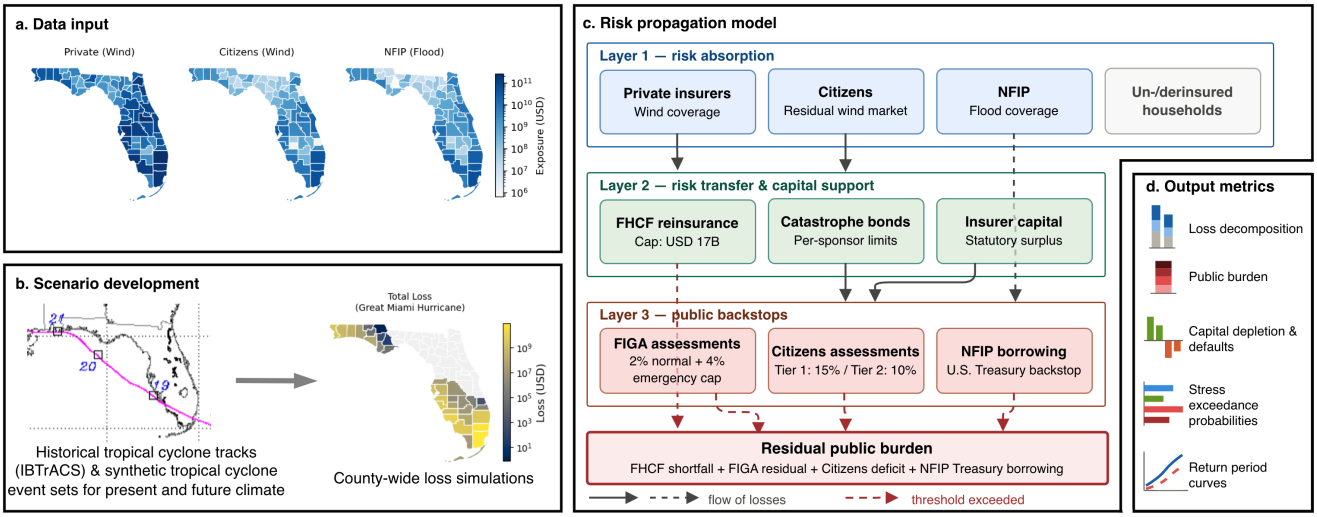

Fig. 1. Insurance system architecture and risk propagation in the Florida homeowners' property insurance market. a) County-level exposure and coverage-in-force for private wind insurers, Citizens Property Insurance Corporation (Citizens), and the U.S. National Flood Insurance Program (NFIP), together with the policy terms, capital positions, and contractual constraints used as model inputs. b) Illustrative example of the hazard-to-loss estimation for a single event: the track of the 1926 Great Miami Hurricane (from IBTrACS; left) is translated into county-level wind and flood loss estimates on 2024 exposure (right). For clarity, only this one historical track is shown; the probabilistic analysis additionally draws on large synthetic tropical cyclone event sets representing present-day and future climate conditions (Methods), which are not displayed here. c) Loss propagation through three sequential layers: (1) risk absorption by private insurers, Citizens, the NFIP, and un-/under-insured households; (2) risk transfer and capital support via the Florida Hurricane Catastrophe Fund (FHCF; statewide seasonal cap USD 17B), catastrophe bonds, and insurer statutory surplus; and (3) public backstops, comprising Florida Insurance Guaranty Association (FIGA) assessments (2% normal plus up to 4% emergency), Citizens' two-tier assessments (Tier 1 up to 15%, Tier 2 up to 10%), and NFIP Treasury borrowing, which together determine the residual public burden. Solid arrows denote the flow of losses; dashed black arrows indicate the flow of losses that bypass one layer; dashed red arrows indicate losses transferred once an institutional threshold or statutory cap is exceeded. d) Main output metrics, color-coded to the model layer in (c) that generates them: loss decomposition, public burden by backstop, insurer capital depletion and defaults, stress exceedance probabilities, and return period curves, evaluated under single, sequential, and probabilistic event scenarios.

Results

Stress testing the insurance system with historical and sequential events

We examine how extreme losses are distributed across households, insurers, and public backstops, using four historically damaging TCs affecting Florida: the Great Miami Hurricane (1926), the Lake Okeechobee Hurricane (1928), Hurricane Andrew (1992), and Hurricane Irma (2017). These four storms span distinct hazard profiles and historical eras, ranging from intense wind over the modern Miami metropolitan area to inland and statewide flooding, and they are among the most damaging TCs in Florida's history. We selected them as recognizable, high-consequence analogues for stress testing. Throughout, these named storms denote stylized stress-test scenarios: each is a historical hazard footprint evaluated on 2024 exposure and insurance market conditions, not a reconstruction of the original event or of its realized losses. To probe how the system responds to temporally clustered events, we also construct sequential scenarios that combine these footprints within a single season: a paired scenario, in which two different storm scenarios occur in succession (Great Miami followed by Andrew), and repeated-event scenarios, in which the same storm scenario occurs twice within the same season (Great Miami twice; Irma twice). Modeled total losses (table S3) fall within the range of published normalized estimates (Supplementary Material Table 2 in Mueller et al., 2025 (49).

Across all scenarios, approximately 60–75% of losses remain uninsured or underinsured (Fig. 2a), with the highest shares occurring in flood-heavy events affecting inland areas with low flood insurance penetration (Fig. 1a, right-most panel). Public burden — residual losses propagated through the insurance system to public institutions after private capital and statutory backstop capacities are exhausted — reaches approximately USD 12 billion for Hurricane Andrew, USD 18 billion for the Lake Okeechobee Hurricane, and USD 26 billion for the Great Miami Hurricane. Sequential events generate public burdens of USD 50–65 billion, exceeding the sum of individual-event burdens: a nonlinear amplification of public costs reflecting institutional thresholds and payout caps. By contrast, Hurricane Irma losses are largely absorbed by the initial insurance layers (public burden of USD 0.2 billion). These differences reflect the magnitude of insured losses reaching the backstops rather than total losses alone. Although Irma's total losses are large, they fell disproportionately on flood-exposed areas of low insurance penetration, so much of the loss remained with uninsured households and only a small residual propagated to the public backstops. Although the FHCF only reaches its statutory cap for Great Miami-scale or sequential events, FIGA, Citizens, and the NFIP accrue deficits in most scenarios that would require multiple years of premium income to recover (table S3, stress ratios).

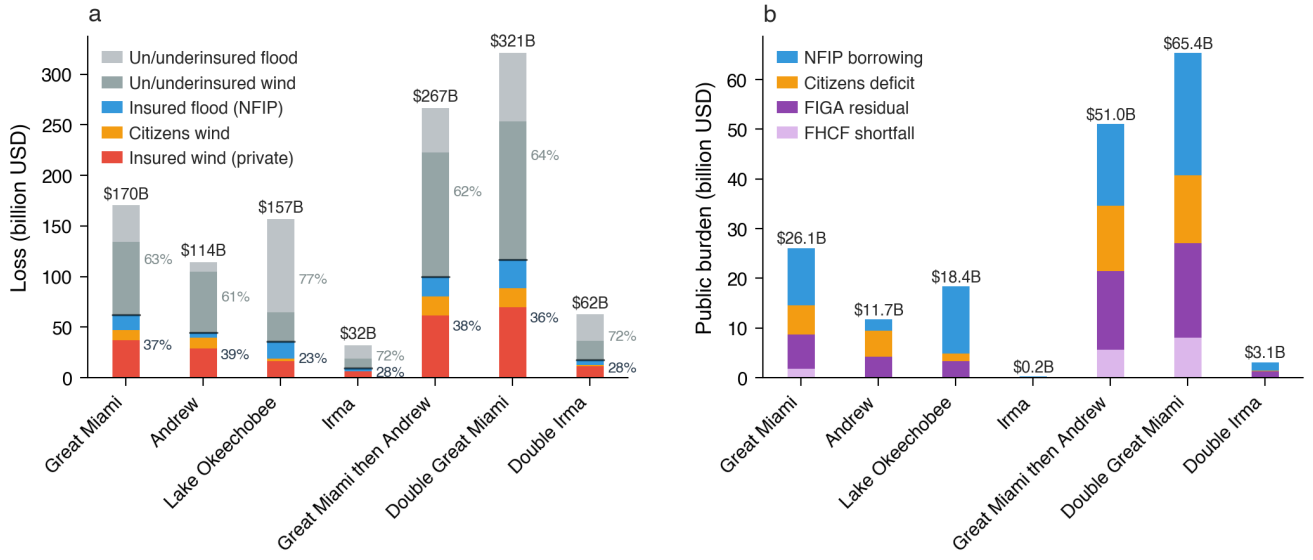

Fig. 2. Loss decomposition and public burden across historical and sequential TC scenarios. a) Decomposition of total losses across insured wind (private market and Citizens), insured flood, and uninsured or underinsured losses. The black horizontal line indicates the split between insured and uninsured losses, with corresponding shares shown numerically. b) Public burden after exhaustion of private insurer capital and risk transfer mechanisms, apportioned across key public backstops. Total loss and public burden values (billion USD) are shown above each bar. All values are shown for single and sequential-event scenarios; a complete tabulation, including uncertainty ranges, is provided in table S3. Named storms denote stylized hazard footprints evaluated on 2024 exposure and insurance market conditions, not reconstructions of the original events or their realized losses.

Probabilistic assessment of systemic insurance risks

Moving beyond individual scenarios, we quantify systemic insurance risk probabilistically using a catalog of 10 000 simulated TC seasons (Section Hazard and loss modeling). Table 1 places the scenario-based stress tests into a probabilistic context by reporting seasonal return period estimates under present-day climate conditions. A total seasonal loss comparable to the Great Miami Hurricane ($\approx$ USD 170 billion) corresponds to a return period of approximately 35 years under present-day climate and exposure, while the sequential-event scenarios examined above approach the magnitude of a 100-year season.

Moreover, the probabilistic results reveal pronounced nonlinear amplification of public burden with increasing loss severity (Fig. 3). For each return period, we compare the estimated total public burden with the corresponding estimate of total seasonal loss. If public burden increased proportionally with total losses, the relationship would follow a constant-share reference line. Instead, public burden rises much more steeply, scaling approximately with the 1.64 power of total loss over the return period range shown. While total seasonal losses increase by approximately a factor of nine between the 10-year and 100-year levels

Table 1. Loss decomposition and public institutional burden across return periods. Return period (RP) estimates are shown for total losses, their decomposition across insured and uninsured components, and the resulting public and quasi-public institutional burden. Public burden reflects residual financial obligations borne by public backstops after exhaustion of private insurer capital and risk transfer mechanisms.

	Return period [years]						
Metric (USD B)	**10**	**25**	**50**	**100**	**250**	**500**	**1000**
Loss decomposition							
Total loss	39.5	146.9	246.4	357.2	563.9	628.0	738.0
Insured wind – private	11.6	41.8	69.7	103.2	155.2	198.4	214.3
Citizens wind	1.8	6.8	14.5	22.1	35.6	53.6	62.9
Insured flood – NFIP	0.9	3.7	7.4	13.7	26.1	37.6	50.3
Un/underinsured wind	19.8	71.8	125.9	183.1	257.6	321.1	392.1
Un/underinsured flood	3.9	15.1	28.4	47.1	87.3	112.7	141.7
Institutional stress							
Total public burden	1.7	13.9	39.6	74.0	127.7	180.9	214.3
FHCF shortfall	0.0	0.0	6.5	13.7	20.8	26.8	29.6
FIGA residual	1.0	9.2	19.2	32.8	54.9	72.8	80.6
Citizens deficit	0.7	4.5	9.9	17.2	29.3	47.3	57.2
NFIP Treasury borrowing	0.0	0.2	4.0	10.3	22.7	34.1	46.8

(USD 39.5 to 357.2 billion), total public burden increases by more than a factor of forty (USD 1.7 to 74.0 billion; Table 1). This supralinear scaling reflects exhaustion of private insurer capital, activation of institutional thresholds, and binding payout caps that shift an increasing share of losses to public and quasi-public backstops in the tail of the distribution. In most seasons, the layered insurance architecture absorbs losses without imposing any public burden: about 86% of simulated seasons carry none, and burden emerges only in more severe seasons, beyond approximately the 7-year return level.

Across return periods, FIGA residuals constitute the largest and fastest-growing component of public burden. In a 100-year season, FIGA residual losses (USD 32.8 billion) account for nearly half of the total public burden, exceeding both Citizens deficits (USD 17.2 billion) and NFIP borrowing (USD 10.3 billion). FIGA remains the dominant channel through which losses enter quasi-public balance sheets across the full range of return periods considered, whereas FHCF shortfalls remain comparatively limited and occur primarily in more extreme seasons.

The probabilistic approach further allows us to assess the annual exceedance probability of systemic risk thresholds that indicate stress across different components of the insurance system (Fig. 4a, table S5). For the private wind insurance market, the annual probability of more than ten insurer defaults is 11.4%, while the probability that the single largest company deficit exceeds USD 1 billion is 7.2%.

For public and quasi-public institutions, the annual probability of exceeding capacity or statutory thresholds differs across entities. The probability that the FHCF reaches its statewide seasonal payout cap is 0.8%, whereas the probabilities of FIGA and Citizens exceeding their respective assessment capacities are 13.6% and 9.5%. For the NFIP, the probability that annual losses exceed twice its annual premium income is 5.0%. These results mirror the scenario-based findings in Fig. 2, highlighting comparatively greater vulnerability of FIGA, Citizens, and the NFIP relative to the FHCF.

Finally, we relate the aggregate public burden to the economic scale of Florida. The annual probability that total public burden exceeds 1% of Florida's GDP is 3.7%, while the probability of exceeding 10% of state GDP is 0.1%.

Systemic risk probabilities increase with climate change

We next evaluate how projected changes in TC hazard alter systemic insurance risk, holding exposure, capital positions, and regulatory parameters at present-day values. Projections span mid-century (2041–2060) and end-of-century (2081–2100) under SSP2-4.5 and SSP5-8.5 emission scenarios. Future changes are estimated using a multi-model delta approach: ensemble-median changes in each risk metric across five CMIP6 simulations are added to the ERA5-based present-day baseline (Section Future climate scenarios). Throughout, the SSP and period labels identify the corresponding GCM-ensemble hazard deltas rather than a specific emissions pathway, since different emissions trajectories can produce similar deltas. The changes reported below therefore isolate the response of the present-day insurance architecture to climate-driven shifts in the TC loss distribution.

Under mid-century scenarios (2041-2060), expected annual total losses approximately double relative to present-day conditions, and expected public burden increases by a factor of approximately three (table S4). Exceedance probabilities of

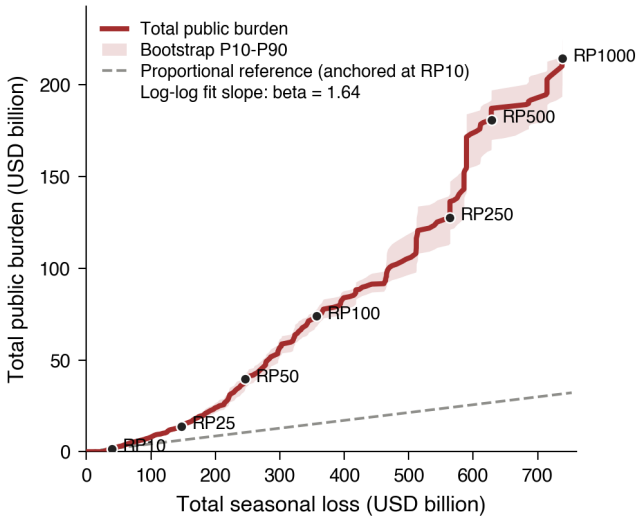

Fig. 3. Supralinear scaling of public burden with seasonal loss. Total public burden plotted against total seasonal loss for present-day climate and the 2024 market configuration, based on 10,000 simulated tropical cyclone seasons. Points show estimates at the return periods (RPs) reported in Table 1. The dashed line shows a proportional, constant-share reference anchored at the 10-year RP; the public burden curve lies above this reference, indicating that public burden increases faster than proportionally with total loss (log-log slope $\beta \approx 1.64$). The plotted RP estimates are marginal quantiles of each metric, as in Table 1, so the curve shows a quantile-quantile relationship rather than paired outcomes from individual simulated seasons. Total public burden is the sum of four institutional components: FHCF shortfall, FIGA residual, Citizens deficit, and NFIP Treasury borrowing. Shading shows the 10th-90th percentile bootstrap interval.

several systemic stress thresholds increase across the private market and post-insolvency channels (Fig. 4, table S5). The annual probability of more than ten insurer defaults rises from 11.4% under present-day conditions to 17.7% (SSP2-4.5) and 18.8% (SSP5-8.5).

Post-default and residual-market mechanisms exhibit particularly strong amplification. The probability that FIGA exceeds its statutory assessment capacity increases from 13.6% to 22.1–23.3%, while Citizens exceeds its assessment capacity with probabilities rising from 9.5% to 15.1–16.1%. In contrast, the probability that the FHCF reaches its statewide payout cap remains at or below 1% across scenarios, and the probability that NFIP annual losses exceed twice premium income increases only modestly (from 5.0% to 5.9–6.1%).

Uncertainty across climate models is substantial but does not alter the qualitative direction of change (table S5). Under 2050 SSP5-8.5, the probability that FIGA exceeds capacity ranges from 16.6% to 30.9% across the GCM ensemble, compared with 13.2–14.1% at baseline, with similar spreads for private insurer defaults and Citizens deficits. Differences between emission scenarios widen by end-of-century but remain smaller than the inter-GCM range. At the aggregate level, the annual probability that total public burden exceeds 1% of Florida's GDP increases modestly from 3.7% to 4.3–4.5% by mid-century, while exceedance of 10% of GDP remains rare.

Systemic risks with evolving markets and insurance policies

We next evaluate how changes in market structure and insurance policies modify systemic risk under present-day hazard conditions. The three stylized interventions represent dynamics currently discussed in policy and industry debates: private market contraction and expansion of residual markets following recent insolvencies and insurer withdrawals (14, 16, 17); expansion of insurance penetration to reduce protection gaps (9); and strengthened building codes and retrofitting initiatives aimed at reducing physical losses (50, 51). Each intervention modifies a distinct layer of the insurance system architecture while holding all other model components constant (Section Stylized market and policy interventions).

Private insurer market exit We model a contraction of the private wind market that increases Citizens' market share from 15% to 25% of total insured value, corresponding to a 10% shift of exposure from private insurers, of which 85% transfers to Citizens and 15% becomes uninsured. Under this scenario, the annual probability of more than ten private insurer defaults

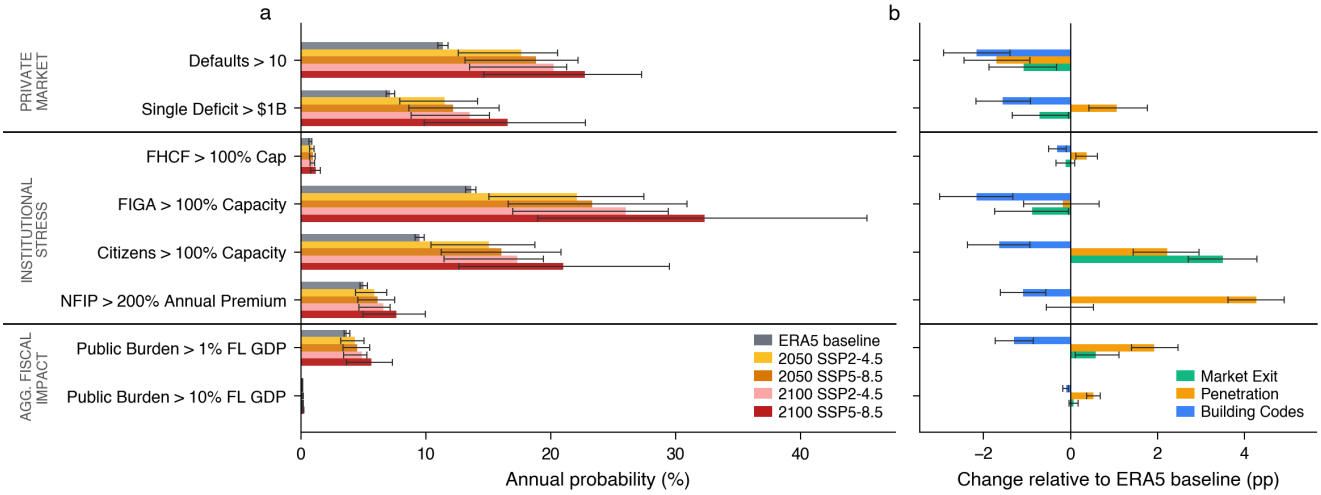

Fig. 4. Probabilistic assessment of systemic insurance risks under future climate scenarios and stylized policy interventions. Annual exceedance probabilities of predefined systemic stress thresholds across the private insurance market (top), public and quasi-public entities (middle), and aggregate fiscal impact measured as total public burden relative to Florida's GDP (bottom). (a) Absolute annual exceedance probabilities under present-day and future climate conditions. Shown are results for the ERA5 baseline climate (grey), mid-century SSP2-4.5 (yellow) and SSP5-8.5 (orange), and end-of-century SSP2-4.5 (pink) and SSP5-8.5 (red). Bars show mean annual exceedance probabilities corresponding to the median climate-induced risk change across the GCMs used for tropical cyclone track set generation (Section Future climate scenarios), based on 10 000 simulated tropical cyclone seasons; error bars indicate the 10th–90th percentile range across the full GCM ensemble. (b) Changes in annual exceedance probabilities relative to the ERA5 baseline configuration under three stylized policy scenarios: private insurer market exit (green), increased insurance penetration (orange), and strengthened building codes (blue). Values represent percentage-point changes under present-day hazard conditions. Bars show mean changes based on 10 000 simulated tropical cyclone seasons, with error bars indicating the 10th–90th percentile. Positive values indicate an increase in the probability of exceeding the corresponding stress threshold relative to baseline; negative values indicate a reduction.

declines by about 1.1 percentage points relative to the ERA5 baseline (Fig. 4b, table S5), reflecting the reduced exposure and insured loss volume within the private market. However, systemic stress shifts toward residual market mechanisms. The probability that Citizens exceeds its assessment capacity increases by about 3.5 percentage points, while exceedance of the FHCF statewide payout cap remains nearly unchanged (table S5). Expected total public burden rises from USD 2.7 billion to USD 3.1 billion (table S4), and the probability that total public burden exceeds 1% of Florida's GDP increases by around 0.6 percentage points (Fig. 4b, table S5).

Insurance penetration increase We increase wind (from 40% to 60%) and flood (from 11% to 30%) penetration rates, with insurer surplus and NFIP premium volumes scaling proportionally to insured exposure. While expanded coverage reduces uninsured losses from USD 12.1 billion (combined wind and flood) under baseline conditions to USD 7.8 billion (table S4), its systemic effects are heterogeneous. Several indicators of stress in public or quasi-public institutions increase under higher insurance penetration. Most notably, the annual probability that NFIP losses exceed 200% of annual premium income increases by 4.3 percentage points relative to the ERA5 baseline (Fig. 4b, table S5), despite the proportional expansion of the premium base — reflecting both the geographic concentration of the new exposure and the supralinear growth of tail losses relative to mean losses under correlated risk. The probability that Citizens exceeds its assessment capacity increases by 2.3 percentage points, and the probability that total public burden exceeds 1% of Florida's GDP increases by 1.9 percentage points (table S5). Expected public burden rises from USD 2.7 billion to USD 5.1 billion (table S4).

In contrast, several indicators of stress within the private insurance market decline. The annual probability of more than ten private insurer defaults decreases by 1.7 percentage points, while FIGA exceedance decreases marginally by 0.2 percentage points (table S5). These patterns indicate that proportional scaling of capital and premium income does not automatically preserve institutional resilience when insured loss volumes increase (Section Stylized market and policy interventions).

Building code improvement We reduce wind-related losses by 30% and flood-related losses by 25% relative to baseline vulnerability before allocation across institutional layers. Exceedance probabilities decline consistently across private, residual,

and public components (Fig. 4b, table S5). The annual probability of more than ten private insurer defaults decreases by 2.2 percentage points relative to the ERA5 baseline, FIGA exceedance decreases by 2.1 percentage points, and Citizens capacity exceedance decreases by 1.6 percentage points. The probability that total public burden exceeds 1% of Florida's GDP declines by 1.3 percentage points (table S5). Expected total public burden decreases from USD 2.7 billion to USD 1.6 billion (table S4). Unlike the redistribution scenarios above, structural mitigation reduces systemic stress simultaneously across all layers of the insurance architecture.

We next quantify the building code-related loss reduction required to offset projected mid-century climate impacts (SSP2-4.5, 2041-2060) and restore systemic risk metrics to their present-day ERA5 baseline values (Fig. 5). For the GCM ensemble median, total public burden declines approximately linearly as assumed wind and flood losses are reduced, returning to its present-day baseline at about 70% combined loss reduction (Fig. 5). Annual total loss responds similarly, whereas insurer defaults respond more nonlinearly, with sharper reductions beyond about 70% loss reduction (Figure S3). Combined wind and flood loss reductions of 70-75% are required to restore systemic risk metrics to baseline. The required reduction is sensitive to hazard uncertainty, ranging from 30-40% under lower-end GCM projections to 75-80% at the upper end.

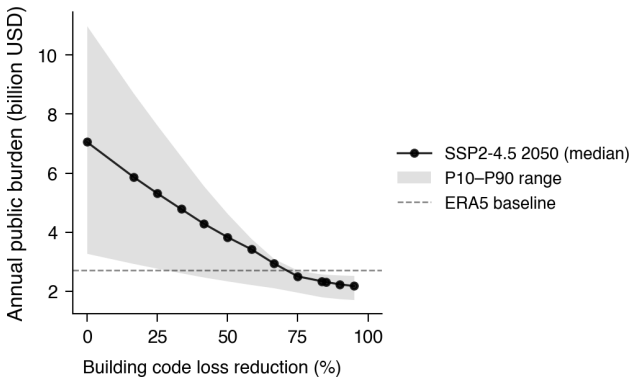

Fig. 5. Sensitivity of public burden estimates to building code–related loss reductions under future climate conditions. Sensitivity analysis showing the effect of incremental reductions in wind- and flood-related losses resulting from strengthened building codes on the estimated total public burdens under mid-century (2041-2060) SSP2-4.5 climate conditions. Solid lines indicate results for the median climate-induced risk change across the GCM ensemble, shaded bands show the 10th–90th percentile range across GCMs, and dashed lines denote the present-day ERA5 baseline. All quantities represent mean annual outcomes across 10 000 simulated tropical cyclone seasons per climate realization. Equivalent results for annual total loss and insurer defaults are shown in Figure S3.

Discussion

Public and quasi-public financial burdens scale disproportionately relative to primary disaster losses as institutional thresholds and capital constraints bind. Across probabilistic simulations of Florida's 2024 insurance market, total seasonal losses increase by approximately a factor of nine between 10-year and 100-year return period seasons, while total public burden increases by a factor of over forty (Table 1, Fig. 3). Previous analyses have suggested nonlinear amplification qualitatively (9); our probabilistic framework quantifies it.

This amplification of public burden is also unevenly distributed across institutions. The highest systemic stress falls on FIGA, followed by Citizens and the NFIP. The annual probability of exceeding institutional capacity or statutory thresholds reaches 13.6% for FIGA and 9.5% for Citizens (Fig. 4a). In contrast, the FHCF remains comparatively resilient across baseline, climate change, and market adaptation scenarios, with a consistently low probability of reaching its statutory cap. The 13.6% annual exceedance probability for FIGA corresponds to approximately a 1-in-7-year frequency of FIGA exhausting its assessment capacity, more than three times more frequent than Andrew-level losses, whose return period under the 2024 Florida market configuration is less than 25 years (Table 1). Both examples are thus matters of immediate concern, not rare tail-risk scenarios.

These modeled frequencies and outcomes are broadly consistent with Florida's recent institutional history. Following the 2004-2005 hurricane seasons, Citizens' assessment capacity was effectively exceeded (16). Its 2005 deficit, on the order of USD 1.7 billion (52), was financed through multi-year post-event bonding and a statewide emergency assessment, together

with a USD 715 million state appropriation (SB 1980; ch. 2006-12, Laws of Florida) (53). More recently, the 2021-2023 wave of insurer insolvencies, in which at least seven residential carriers entered liquidation, triggered successive FIGA assessments: a 0.70% assessment in 2021, a 1.3% and a further 0.70% assessment in 2022, and a 1.0% multi-year emergency assessment in 2023 (47). Over the same period, the FHCF drew down its reserves but did not breach its statutory reimbursement cap. This ordering, namely, the recurrent binding of the FIGA and Citizens mechanisms along with a resilient FHCF, mirrors the relative exceedance probabilities our study produces (FIGA 13.6%, Citizens 9.5%, FHCF 0.8%). Of the storms we model, Hurricane Irma (2017) is the most recent, and the only one to occur after all the institutions we represent (Citizens, NFIP, FHCF, and FIGA) were in place, so it offers the one direct comparison. Irma was absorbed within the insurance system, with no Citizens special assessment and no exhaustion of the FHCF, in line with the small public burden of our Irma scenario (USD 0.2 billion; Table S3). These comparisons span different market configurations, and the insolvency-driven cases reflected litigation and reinsurance costs as well as catastrophe losses. We therefore present them as qualitative corroboration that the modeled probabilities and outcomes are plausible, not as a formal out-of-sample validation.

Our results place the annual probability that public burden from hurricanes exceeds 1% of Florida's output at 3.7% (about once in thirty years), and the probability that it exceeds 10% at 0.1% (about once in a thousand years). To put these magnitudes in perspective, the largest comparable public costs in the financial stability literature are those of banking crises: when a banking system fails, governments commit public funds to stabilize it, for example by recapitalizing failing banks as in 2007-2009. Across systemic banking crises in advanced economies since 1970, this fiscal cost has a median of about 7% of GDP, or 3% once later recoveries are netted out (54). Because Florida's annual economic output was about USD 1.7 trillion in 2024, a burden expressed as a share of state output is comparable to these national figures (55). A public burden of a few percent of output, comparable to a typical banking crisis bailout, therefore arises in our study on the order of once a century, while the rarest seasons produce public burdens above 10% of output, exceeding the fiscal cost of a typical banking crisis. Climate-driven insurance losses, from a single state and a single hazard, can thus reach the fiscal scale that financial stability analysis associates with systemic banking events.

Because climate change, market structure, and policy interventions are evaluated within the same architecture, their effects propagate through the entire insurance system. Increasing insurance penetration with proportional capital expansion, for example, reduces private insurer stress but raises public backstop exposure: the annual probability that NFIP losses exceed 200% of annual premium income rises by 4.3 percentage points, and Citizens capacity exceedance rises by 2.3 percentage points (Section Insurance penetration increase). Policies targeting one component of the insurance market can thus redistribute systemic risk across institutions rather than uniformly reducing it.

The market dynamics and policy interventions examined here are stylized and designed to probe systemic sensitivity rather than forecast specific outcomes. Empirical evidence suggests that conventional building codes reduce wind damage. After Florida's 2001 code revision, homes built to the updated code were about 22% less likely to sustain wind damage and showed approximately 27% lower damage severity (50). The enhanced, voluntary FORTIFIED standard performs substantially better, reducing insured loss frequency by 55-74% and loss ratios by 51-72% in Hurricane Sally (56). Offsetting the projected mid-century (2050, SSP2-4.5) increase in systemic risk requires loss reductions of about 70-75% under the median hazard scenario, falling to 30-40% under lower-end projections (Fig. 5); this range in future climate outcomes reflects differences in climate sensitivity across the underlying GCMs (57). Because these empirical estimates refer to wind damage and insurance claims from individual events, they are not directly comparable to our system-level sensitivity, which represents the combined wind-and-flood loss reduction required to restore present-day stress probabilities. As benchmarks, however, they suggest that conventional code improvements fall well short of the loss reduction required to offset median mid-century climate impacts, while the strongest documented standard delivers substantially larger reductions but remains voluntary and not yet widely adopted. Reliance on a single structural measure is therefore unlikely to suffice under stronger warming; strengthening insurance market resilience will likely require a portfolio of complementary policy and market interventions.

Several simplifications bound the interpretation of these results, and the majority of them bias the framework toward overstating rather than understating systemic stress (table S8). Disaggregating statewide private insurer market shares uniformly to counties, in the absence of insurer-specific county data, tends to overstate the number of simultaneous insurer defaults and the size of FIGA assessments. Representing the FHCF as the only reinsurance mechanism omits private reinsurance, which would otherwise reduce net retained losses and, in turn, modeled defaults and FIGA assessments. The indirectly calibrated wind insured fraction, approximately 40% in severe events, may overstate coverage in smaller events, although it aligns with observed take-up in the large-loss years that dominate systemic risk outcomes (Supplementary Methods). The 1980-2023 hazard baseline likewise tends toward somewhat higher modeled losses than industry event catalogs calibrated to longer historical records, consistent with the sensitivity of Atlantic hurricane risk estimates to baseline-period choice (49, 58, 59). Taken together, these choices imply that our reported magnitudes are best interpreted as upper bounds, whereas the qualitative conclusions, the supralinear amplification of public burden and its concentration in FIGA, Citizens, and the NFIP rather than the FHCF, are

stable across the climate scenarios and the input ranges we vary (tables S6 and S7). The principal simplification acting in the opposite direction is the omission of sea-level rise, which likely leads us to underestimate long-term flood-related systemic risk.

A second group of limitations concerns the scope of the analysis. The framework is applied to Florida and to TCs alone. Wind and flood losses are partitioned with an external multi-hazard regression that is suitable for system-level probabilistic stress testing but not for event-level attribution. For future climate scenarios, the 2024 market architecture is held fixed, so projected stress should be read as a conditional assessment of the present-day configuration rather than a forecast of how the market will evolve.

By embedding probabilistic hazard realizations within a market-wide representation of insurer capitalization and public backstops, this study provides a quantitative framework for evaluating how climate-driven disaster losses propagate through insurance systems. Our results show that systemic financial exposure can increase nonlinearly with disaster losses, concentrate within specific public backstop institutions, and shift across actors in response to policy and market changes. These findings suggest that insurance market stability should be evaluated not only in terms of institutional solvency, but also in terms of whether the system reduces underlying risk, preserves access to recovery finance, and limits the transfer of losses to households, policyholders, and public institutions.

Beyond Florida, the framework developed here provides a template for stress testing other climate-exposed insurance markets. California's wildfire-prone regions (60) reflect the same layered risk transfer vulnerabilities shown here, and similar risk transfer markets govern disaster insurance internationally. A key priority for future research is to trace how uninsured losses propagate into housing markets, credit systems, and public finance, where emerging evidence points to climate-driven debt feedbacks at the municipal level (61) and persistent protection gaps across U.S. flood markets (62). More broadly, system-wide stress testing can help compare policy choices, including land-use restrictions, insurance affordability measures, public backstops, and structural risk reduction, by evaluating whether they reduce underlying losses or mainly redistribute them across households, policyholders, insurers, and public institutions. Developing integrated tools that connect physical risk, insurance market structure, household protection gaps, and public finance will be essential for managing climate risk as disaster losses increasingly propagate beyond the insurance sector.

Methods

Data

Insurance market data

Insurance market inputs are anchored to statutory and financial conditions as of 2024, based on insurer statutory filings, regulatory reports, and administrative exposure datasets. Exposure and capital data are harmonized to the county level to ensure consistency with aggregated TC loss estimates and are held constant across simulations. This county resolution matches the level at which the modeled institutions (the FHCF, FIGA, Citizens, and the NFIP) assess and pay, and is therefore appropriate for a system-level stress test; finer, property-level data would sharpen individual insurer default estimates without altering the institutional thresholds that drive the systemic results. Table S8 sets out, for each component of the framework, the ideal data a supervisory implementation could use, the public proxy or model adopted here, and the resulting direction of bias. A consolidated list of model parameters, their sources, and their treatment as fixed, stochastically sampled, or varied across the climate ensemble is provided in table S9.

Exposure and coverage For the private admitted market, total insured value (TIV) by county is obtained from the Florida Hurricane Catastrophe Fund (FHCF) 2024 annual exposure report (43), which provides aggregate residential wind exposure across all participating private insurers. To assign this county-level private TIV to individual insurers, we disaggregate it across the top 100 individual insurers in proportion to their statewide residential direct premiums written for calendar year 2024, as reported in statutory filings (NAIC annual statements, accessed via S&P Capital IQ) and Florida Office of Insurance Regulation (FLOIR) statewide market share reports (63). This procedure preserves observed statewide market structure while ensuring consistency with county-level loss aggregation. Insurer-specific county-level exposure is not publicly available: such data are withheld as a trade secret, a position upheld in Office of Insurance Regulation v. State Farm Florida Insurance Co. (226 So. 3d 853, Fla. 1st DCA 2017) (64). We therefore distribute each carrier's statewide share uniformly across counties, which removes the geographic specialisation of individual insurers and yields upper-bound estimates of the number of simultaneous defaults and FIGA assessments (table S8; see Discussion).

Citizens Property Insurance Corporation's (hereafter, "Citizens"') county-level wind exposure is obtained directly from its published policies-in-force and exposure data as of September 30, 2024 (40). We include all personal residential policy lines, comprising multiperil homeowners and wind-only residential policies.

Flood exposure is based on National Flood Insurance Program (NFIP) coverage-in-force and written premium data for policy year 2024, obtained from the Federal Emergency Management Agency (FEMA) OpenFEMA datasets (41). NFIP participation rates reflect observed take-up inside and outside Special Flood Hazard Areas (SFHAs) (65).

Capital and surplus Private insurer capital is measured as statutory surplus as regards policyholders for calendar year 2024, obtained from statutory financial statements filed with the National Association of Insurance Commissioners (NAIC) and accessed via S&P Capital IQ. For insurers affiliated with larger groups, both entity-level and group-level surplus are recorded to allow for potential intragroup capital support within the risk propagation model (Section Capital depletion and intragroup support).

Citizens' surplus as regards policyholders corresponds to its 2024 annual statutory financial statement (66).

NFIP capital consists of the combined National Flood Insurance Fund and Reserve Fund balance of USD 3.441 billion as of October 28, 2024 (CRS Insights IN10784 (45)). Florida-specific annual written premium for policy year 2024, obtained from FEMA OpenFEMA data (41), is used to define exceedance thresholds relative to annual premium income (Section Output metrics and stress indicators).

Reinsurance contracts and catastrophe bond data FHCF contract parameters are based on the 2023-2024 reimbursement contract year. Company-specific coverage elections (45%, 75%, or 90%), reimbursement premiums, and participating insurer identifiers (NAIC codes) are obtained from FHCF coverage selections and premium calculation reports (43). Retention multiples and coverage limits follow the statutory terms reported in the FHCF 2023-2024 annual report (42). Recoveries are subject to the FHCF's season-wide statutory capacity limit of USD 17 billion. The FHCF is modeled as the only reinsurance mechanism explicitly represented; private reinsurance not captured here could reduce modeled defaults and FIGA assessments.

Outstanding catastrophe bonds covering Florida wind exposure active during the 2024 hurricane season are identified using the Artemis deal directory (44) and verified against sponsor offering documents and transaction disclosures. For each bond, we extract sponsor, peril coverage, trigger type (indemnity, industry loss, or parametric), attachment point, exhaustion point, and limit. Bonds are modeled as single-occurrence, single-season layers without reinstatements. Payouts are computed at the sponsor level based on reported attachment and exhaustion terms.

Tropical cyclone track data

We use TC track data from two sources. Historical TC tracks are obtained from the International Best Track Archive for Climate Stewardship (IBTrACS) (37). Synthetic TC tracks are generated using the statistical-dynamical MIT TC model (38, 39).

The model is forced with large-scale environmental fields from the European Centre for Medium-Range Weather Forecasts (ECMWF) fifth-generation reanalysis (ERA5) (67) for present-day conditions and from five CMIP6 global climate models (GCMs) for future conditions under SSP2-4.5 and SSP5-8.5 emission scenarios. The GCMs (CanESM5 (68), CNRM-CM6-1 (69), EC-Earth3 (70), IPSL-CM6A-LR (71), and MIROC6 (72)) span a broad range of global climate sensitivities. Simulations cover three periods: a present-day reference (1980-2023 for ERA5; 1995-2014 for GCMs), mid-century (2041-2060), and late-century (2081-2100). The model was used to generate 200 TCs for each year within these periods using the three-step process of genesis, track, and intensity modeling, yielding a total of 8800 (ERA5) and 4000 (per GCMs) TCs per event set. Annual TC frequency emerges from the fraction of TC seeds used in the genesis step that develop into fully formed storms (>40 kn) under the prevailing environmental conditions (e.g., potential intensity, vertical wind shear). A frequency bias correction rescales the number of developed storms relative to the seeded ensemble, ensuring that simulated annual TC counts match the calibrated climatological baseline while preserving climate-driven variability across simulations. This frequency information is used to generate stochastic year sets (Section Hazard and loss modeling) and compute return periods (Section Output metrics and stress indicators).

To focus on Florida-relevant impacts, we retain only TC tracks passing within a 150 km coastal buffer of Florida.

Hazard and loss modeling

We compute county-level TC loss estimates from historical and synthetic TC tracks using the open-source, probabilistic climate risk modeling platform CLIMADA (73), which operationalizes the IPCC risk framework based on hazard, exposure, and vulnerability (74).

First, we use the Holland (2008) (75) parametric wind model to derive a two-dimensional wind field at a horizontal resolution of 120 arc-seconds (approximately 4 km at the equator) from each TC track. The wind model produces the gridded 1-min average sustained winds at 10 m above ground, consisting of a circular wind field component and the translational wind speed generated by the TC's movement. In CLIMADA, the peak lifetime wind speed at each location is used as the hazard variable, disregarding values below 34 kn (17.5 $\mathrm{m\,s^{-1}}$). We do not explicitly model TC rainfall or storm surge hazards; their

relative contribution to total losses is incorporated through the wind-flood attribution approach described below (Section Wind and flood loss estimation). Sea-level rise projections are not included in future climate TC hazard sets.

Second, we derive a spatially explicit representation of gridded asset exposure values based on the LitPop method (76), which disaggregates national or subnational GDP values to a grid level based on nightlight intensity and population data. The Florida exposure layer used in this study is computed at a resolution of 120 arc-seconds using GDP values (in USD) from 2020.

Third, we use regionally calibrated impact functions (also called vulnerability functions) that relate hazard intensities to relative economic damage ratios (77) to compute event-based loss estimates. The regional calibration was conducted for nine global regions of differing socio-demographic composition and vulnerability. Here, we apply the USA-specific impact function to represent macroeconomic TC losses at the state scale; sub-county variations in structural vulnerability are not explicitly modeled, consistent with the system-level focus of this analysis. Although parameterized by wind intensity, the impact functions were calibrated to observed total TC losses and therefore capture the aggregate effects of wind, rainfall, and storm surge.

The resulting total loss estimates for historical TCs (1926 Great Miami Hurricane, 1992 Hurricane Andrew, 1928 Lake Okeechobee Hurricane, and 2017 Hurricane Irma; table S3) fall within the range of normalized loss estimates reported in the literature (Supplementary Material Table 2 in Mueller et al., 2025 (49).

For the historical scenario-based insurance market stress test, we construct sequential-event scenarios by combining individual TCs: Great Miami followed by Andrew, Great Miami twice, and Irma twice. Losses are computed sequentially to account for reductions in exposed asset values after the first event. We do not model potential changes in vulnerability between events due to limited empirical evidence. These sequential scenarios should therefore be interpreted as stylized stress tests that capture exposure depletion but do not incorporate additional compounding or dynamic recovery effects. The TC hazard model uses a baseline period of 1980-2023 (38, 39). Because Atlantic hurricane activity exhibits substantial multidecadal variability, estimates calibrated to a shorter recent baseline may differ from those based on longer-term climatologies extending back to the early twentieth century (49, 58, 59). Such baseline period choices can also propagate into downstream loss estimates when hazard-frequency changes are translated through event loss tables or related financial risk models (78). Sea-level rise is not explicitly modeled, implying that long-term systemic risks may be conservatively estimated.

Because the insurance market operates on county-level exposure portfolios, event-based gridded losses are aggregated to county totals, which form the direct input to the financial risk propagation model (Section Insurance market data).

Loss estimates from the synthetic TCs are used to construct stochastic event sets spanning 10 000 simulated years. From the 8800 ERA5-based and 4000 GCM-based simulated events in each TC event set, annual TC seasons are generated by sampling events with replacement according to the TC event set-specific annual frequency (Section Tropical cyclone track data). This procedure yields years without TC losses (ERA5 baseline: 28.5%), years with a single event (15.3%), and years with multiple events (56.2%). Here, "events" refers to all retained synthetic tracks passing within the 150 km Florida coastal buffer (Section Tropical cyclone track data), including storms that produce limited or spatially confined county-level losses. These synthetic year sets form the basis of the probabilistic systemic risk assessment.

Wind and flood loss estimation Because the systemic stress test requires separate accounting of wind and flood losses within the insurance market structure (Section Layer 1: Risk absorption), total TC losses must be decomposed into sub-hazard components. Explicit simulation of rainfall- and surge-driven losses using dedicated hazard models would be computationally intensive and require additional impact-function calibration and multi-peril loss modeling, for which event-level empirical data separating wind and flood damages remain limited. Instead, we adopt a pragmatic and physically informed wind-flood attribution approach based on an external multi-hazard damage regression model. This regression-based attribution is designed for system-level probabilistic stress testing rather than event-level loss attribution.

Specifically, we partition total economic TC losses simulated in this study (Section Hazard and loss modeling) into wind and flood components using the multi-hazard regression model of Gori et al. (2025) (79, 80). That study combines county-level wind, rainfall, and storm surge intensities derived from physics-based hazard models with a regression-based damage model calibrated on observed disaster losses. Because the TC simulations in Gori et al. (2025) are based on the same underlying statistical-dynamical TC track model used here (38, 39), their hazard dataset provides a consistent basis for estimating relative wind and flood contributions.

For each TC event e and county c, we define log-space hazard contributions following the damage function of Gori et al. (2025):

$$c_{V,e,c} = \beta_V \ln V_{\max,e,c}, \qquad c_{P,e,c} = \beta_P \ln(P_{\mathrm{cum},e,c} + 1), \qquad c_{S,e,c} = \beta_S S_{\max,e,c}, \tag{1}$$

where $V_{\max}$, P_{cum}, and $S_{\max}$ are maximum wind speed, cumulative precipitation, and maximum surge, respectively, and regression coefficients β_V, β_P, and β_S follow the regional specification of Gori et al. (2025) (79). The compound hazard intensity is

$$H_{e,c} = c_{V,e,c} + c_{P,e,c} + c_{S,e,c}. \tag{2}$$

To focus on high-intensity hazard realizations most relevant for systemic loss and insurance stress, we restrict the analysis to events exceeding the county-specific 95th percentile threshold $H_c^{(p95)}$, computed independently for each county across all modelled events. Within this subset, we compute the county-level wind attribution as the mean of the per-event contribution ratios:

$$\tilde{r}_{V,c} = \left\langle \frac{c_{V,e,c}}{c_{V,e,c} + c_{P,e,c} + c_{S,e,c}} \right\rangle_{H_{e,c} \geq H_c^{(p95)}}. \tag{3}$$

Aggregation across Florida's exposure-weighted counties yields a state-wide wind attribution of 84.6% (flood: 15.4%, comprising 10.2% surge and 5.2% precipitation).

For each simulated event, an event-level wind share is sampled from a Beta prior (event-specific for historical benchmark events; otherwise from a default prior centered at 84.6% wind). Total county loss is then partitioned into wind and flood components using county-specific wind shares $\tilde{r}_{V,c}$, after proportional rescaling so that the loss-weighted state-wide mean exactly equals the sampled event-level wind share. Flood loss is defined residually as the complement of wind loss.

$$L_{V,e,c} = L_{\text{total},e,c}\, r_{V,e,c}, \qquad L_{F,e,c} = L_{\text{total},e,c}\,(1 - r_{V,e,c}). \tag{4}$$

Here, $r_{V,e,c}$ denotes the rescaled, event-specific county wind fraction derived from $\tilde{r}_{V,c}$.

For the historical benchmark scenarios (1926 Great Miami Hurricane, 1992 Hurricane Andrew, 1928 Lake Okeechobee Hurricane, and 2017 Hurricane Irma), the event-level prior means are set from literature-based damage reconstructions (70%, 87.5%, 30%, and 50%, respectively), with Beta priors used to represent epistemic uncertainty.

Risk propagation model

The risk propagation model translates county-level wind and flood losses into entity-specific financial impacts through the three layers introduced in Section Insurance system architecture and risk propagation (Fig. 1c). Losses are reallocated at each step according to observed exposure shares, contractual terms, statutory limits, and capital positions (Section Insurance market data); the same logic is applied to every event and every simulated season. The following sections provide the quantitative specification of each layer and the simulation design. Throughout, we suppress the event index for readability; all quantities are evaluated separately for each event or simulated season.

Layer 1: Risk absorption

The hazard and loss model yields total economic losses (Section Hazard and loss modeling), which are mapped onto the residential insurance system in the risk propagation model rather than during the loss modeling step. For each county c, gross wind and flood losses $L_{W,c}$ and $L_{F,c}$ are split into insured and uninsured components.

The insured wind fraction f_W is sampled per iteration from a Beta$(4,6)$ distribution (mean 0.40), calibrated to observed Florida residential insurance experience (Supplementary Methods). Insured wind losses are

$$L_{W,c}^{\text{ins}} = f_W\, L_{W,c}, \qquad L_{W,c}^{\text{hh}} = (1 - f_W)\, L_{W,c}, \tag{5}$$

where the residual $L_{W,c}^{\text{hh}}$ is retained by uninsured or underinsured households and does not enter the insurance system. Insured wind losses are allocated to the private admitted market and Citizens by their county-level TIV shares, and the private share is distributed across insurers i in proportion to their county TIV $v_{i,c}$:

$$G_i = \sum_c \frac{v_{i,c}}{V_c^{\text{priv}}}\, \sigma_c\, L_{W,c}^{\text{ins}}, \qquad G_{\text{Cit}} = \sum_c \left(1 - \sigma_c\right) L_{W,c}^{\text{ins}}, \tag{6}$$

where σ_c is the private market's share of insured wind value in county c and $V_c^{\text{priv}} = \sum_i v_{i,c}$.

Insured flood losses are set directly from observed county NFIP take-up τ_c (insurance penetration), capped by aggregate coverage-in-force CIF_c, and assigned to the NFIP:

$$L_{F,c}^{\text{ins}} = \min\left(\tau_c\, L_{F,c},\ \text{CIF}_c\right), \qquad L_{F,c}^{\text{hh}} = L_{F,c} - L_{F,c}^{\text{ins}}. \tag{7}$$

Federal disaster assistance does not enter the flood calculation. These allocations establish each entity's gross insured loss before reinsurance recoveries or capital adjustments.

Layer 2: Risk transfer and capital support

FHCF reinsurance. Each insurer i holds an FHCF contract with reimbursement premium Π_i and coverage election $p_i \in \{0.45, 0.75, 0.90\}$. Its retention and per-company limit are

$$R_i = m_{\text{ret}}(p_i)\,\Pi_i, \qquad K_i = m_{\text{pay}}\,\Pi_i, \tag{8}$$

with $m_{\text{ret}}(0.90) = 6.0732$, $m_{\text{ret}}(0.75) = 7.2878$, $m_{\text{ret}}(0.45) = 12.1464$, and payout multiple $m_{\text{pay}} = 11.2368$ (2023-24 contract terms). The recovery applies the coverage election p_i and the loss-adjustment-expense factor $\lambda = 1.10$ to the retained excess, which is first capped at the per-company limit K_i:

$$\text{Rec}_i = \lambda\, p_i \min\Big(\max\big(G_i - R_i, 0\big),\, K_i\Big). \tag{9}$$

Aggregate recoveries are constrained by the statewide seasonal cap $C_{\text{FHCF}} = \$17$ billion. We denote the cap-adjusted recovery by $\widetilde{\text{Rec}}_i$: if $\sum_i \text{Rec}_i > C_{\text{FHCF}}$, individual recoveries are scaled proportionally, $\widetilde{\text{Rec}}_i = \text{Rec}_i\, C_{\text{FHCF}} / \sum_j \text{Rec}_j$; otherwise $\widetilde{\text{Rec}}_i = \text{Rec}_i$. The uncovered remainder $F_{\text{FHCF}} = \max\big(\sum_i \text{Rec}_i - C_{\text{FHCF}}, 0\big)$ is recorded as the FHCF component of public burden, and post-FHCF net wind loss is $N_i^{\text{F}} = G_i - \widetilde{\text{Rec}}_i$.

Catastrophe bonds. Catastrophe bonds are modeled as single-occurrence covers within a single season, without reinstatement. For an indemnity bond with attachment A_i and limit Lim_i,

$$B_i = \min\Big(\max\big(N_i^{\text{F}} - A_i, 0\big),\, \text{Lim}_i\Big), \tag{10}$$

while index- or industry-trigger bonds are evaluated on statewide insured wind losses prior to FHCF recovery. Catastrophe-bond payouts reduce insurer net losses but do not modify FHCF mechanics. The net wind loss carried into capital is $N_i = N_i^{\text{F}} - B_i$.

Capital depletion and intragroup support. Net wind losses are applied to each insurer's statutory surplus S_i, giving post-loss surplus $E_i = S_i - N_i$; an insurer is provisionally insolvent if $E_i < 0$. Insurers are grouped at the NAIC parent level. A provisionally insolvent entity is eligible for intragroup support only if it belongs to a group g whose group-to-entity surplus ratio exceeds 10. For each group, the available support pool is the group's excess capital plus the positive surplus of its solvent members,

$$P_g = \max\Big(S_g^{\text{grp}} - \textstyle\sum_{i\in g} S_i,\; 0\Big) \;+\; \sum_{i\in g} \max(E_i, 0). \tag{11}$$

Eligible deficits are cured up to non-negative surplus, funded from the parent pool first and then from solvent members in proportion to their surplus, without pushing any supporter below zero and subject to P_g. Writing the resulting contribution to entity i as $C_i \geq 0$, the adjusted surplus and default status are

$$E_i' = E_i + C_i, \qquad \text{entity } i \text{ defaults if } E_i' < 0. \tag{12}$$

NFIP. NFIP-insured flood payouts first draw on the national fund pool $P_{\text{NFIP}} = \$3.441$ billion; the excess is recorded as U.S. Treasury borrowing,

$$\text{NFIP}_{\text{borrow}} = \max\Big(\textstyle\sum_c L_{F,c}^{\text{ins}} - P_{\text{NFIP}},\; 0\Big). \tag{13}$$

Layer 3: Public and quasi-public backstops

Residual losses that exhaust private capital and Layer-2 financing are allocated to three statutory channels.

FIGA. The aggregate deficit of defaulted insurers, $D_{\text{FIGA}} = \sum_{i:E_i'<0}\big(-E_i'\big)$, is met by assessments on surviving insurers' written premium Π_{surv} up to 2% normal plus 4% emergency:

$$F_{\text{FIGA}} = \max\big(D_{\text{FIGA}} - 0.06\,\Pi_{\text{surv}},\; 0\big). \tag{14}$$

Citizens. Citizens' gross wind loss passes through the same Layer-2 risk transfer as private insurers, yielding net wind loss N_{Cit}, which is applied to its surplus, $D_{\text{Cit}} = \max(N_{\text{Cit}} - S_{\text{Cit}}, 0)$; any remaining deficit is met by two assessment tiers: Tier 1 up to 15% of Citizens' premium base Π_{Cit}, then Tier 2 up to 10% of the statewide property premium base Π_{state}:

$$T_1 = \min\big(D_{\text{Cit}},\; 0.15\,\Pi_{\text{Cit}}\big), \tag{15}$$

$$T_2 = \min\big(D_{\text{Cit}} - T_1,\; 0.10\,\Pi_{\text{state}}\big), \tag{16}$$

$$F_{\text{Cit}} = \max\big(D_{\text{Cit}} - T_1 - T_2,\; 0\big). \tag{17}$$

Total public burden.

$$B_{\text{public}} = F_{\text{FHCF}} + F_{\text{FIGA}} + F_{\text{Cit}} + \text{NFIP}_{\text{borrow}}. \tag{18}$$

Simulation design and probabilistic metrics

The model is evaluated in two settings. Event-based stress tests apply the model to individual historical events and constructed sequential scenarios with 200 Monte Carlo iterations each, capturing parametric uncertainty while holding the event fixed. The probabilistic assessment uses $N = 10{,}000$ synthetic TC seasons, each representing a stochastic realization of annual TC occurrence and associated parameters. Sampled parameters are the insured wind fraction ($\text{Beta}(4,6)$), the event-level wind/flood share (Beta priors; Section Wind and flood loss estimation), and a $\text{CoV} = 0.15$ perturbation of county TIV; all other parameters are held at 2024 statutory values. For an exceedance condition $\mathscr{B}$, the annual exceedance probability is

$$P(\mathscr{B}) = \frac{1}{N}\sum_{j=1}^{N} \mathbf{1}[\mathscr{B}_j], \tag{19}$$

and empirical return periods are the inverse of the ranked cumulative exceedance frequency. Future-climate values are obtained by adding GCM-ensemble hazard deltas to the ERA5 baseline (Section Future climate scenarios).

Output metrics and stress indicators

Model outcomes are evaluated using metrics designed to quantify (i) loss decomposition across primary risk absorption entities, (ii) institutional stress within the insurance system, (iii) capital depletion and default dynamics, and (iv) system-level fiscal impacts. Formal definitions of all metrics are provided in table S2.

For each event or simulated season, total economic losses are decomposed into insured wind losses (private insurers and Citizens), insured flood losses (NFIP), and uninsured household losses. This decomposition characterizes the insurance protection gap and the initial distribution of gross damages across households, insurers, and public or quasi-public institutions.

Institutional stress for public and quasi-public entities is quantified relative to their binding statutory or contractual limits as implemented in the risk propagation model. For each event or simulated season, we report realized institutional stress totals (FHCF reimbursements, FIGA deficits, Citizens assessment utilization, and NFIP borrowing). Within the probabilistic simulations, we additionally compute annual exceedance probabilities of key capacity thresholds, including the FHCF seasonal aggregate cap (USD 17 billion), FIGA's maximum assessment capacity (2% normal plus up to 4% emergency assessments of surviving property insurers' written premium), Citizens' combined Tier 1 (15% of Citizens premium base) and Tier 2 (10% of statewide property premium base) assessment authority, and NFIP insured losses exceeding twice its annual premium income. All parameters reflect 2024 statutory conditions and are held constant across simulations.

private sector stress is measured through post-loss surplus positions after reinsurance recoveries, catastrophe bond payouts, and potential intragroup capital support. We record the number of insurer insolvencies and the largest single-entity deficit. These indicators capture the extent to which losses exceed available private capital buffers.

At the system level, we define total residual public burden as the aggregate fiscal exposure that remains after private capital buffers and statutory institutional capacities are exhausted. This measure combines FHCF reimbursement shortfalls, FIGA and Citizens deficits beyond assessment authority, and NFIP borrowing requirements. We compute annual exceedance probabilities of total public burden relative to Florida state GDP (e.g., $> 1\%$ and $> 10\%$) and derive empirical return periods for total losses and aggregate public-sector burdens across simulated year sets.

Empirical return periods (defined in Section Risk propagation model) are computed separately for the two settings: for seasonal analyses, frequencies correspond to simulated year sets (10 000 stochastic seasons); for event-based analyses, they reflect the modeled annual frequency of individual storms (Section Hazard and loss modeling). The seasonal and event-based return period curves coincide closely (Figure S1), so seasonal aggregation does not materially affect tail-loss frequencies.

Climate change and insurance market configuration experiments

Future climate scenarios Future TC projections are generated using the statistical-dynamical MIT TC model (38, 39) forced by environmental fields from CMIP6 global climate models (Section Tropical cyclone track data). We then evaluate how projected changes in TC activity translate into systemic insurance risk using a multi-model ensemble approach. Rather than using GCM-driven simulations directly to estimate future risk levels, we add climate change deltas to the ERA5 baseline. This delta approach, which is standard in the climate impact literature, avoids systematic low biases in TC intensity that arise when synthetic storms are generated from the lower-resolution environments of global climate models (39, 81).

For each GCM, scenario, time period, and metric, we compute the absolute climate delta as the difference between the future value and that GCM's historical reference value (1995-2014). Deltas are aggregated across the five-GCM ensemble (median and 10th-90th percentile range) and added to the ERA5-based baseline value. Continuous metrics and empirical exceedance probabilities are treated identically: both are computed as annual means within each GCM/scenario simulation (10 000 synthetic years), so the same additive scaling applies uniformly without a separate transformation. This formulation isolates the modeled climate change signal while preserving the observationally constrained baseline distribution derived from ERA5-driven simulations.

Uncertainty in future projections reflects both baseline sampling variability and inter-GCM spread in climate deltas. Baseline Monte Carlo uncertainty is quantified via bootstrap resampling (1000 iterations) of the 10 000-year ERA5 simulations, yielding 10th-90th percentile confidence intervals. Climate change uncertainty is represented by the 10th-90th percentile range of deltas across the five GCMs. These uncertainty bounds are propagated consistently to all reported future risk metrics.

The 2024 market architecture is held fixed across future climate scenarios, isolating the interaction between changing hazard conditions and current institutional structures without accounting for adaptation in underwriting practices, capitalization, or exposure patterns. Future stress estimates should therefore be interpreted as conditional assessments of the present-day market configuration rather than forecasts of how the market will actually evolve.

Stylized market and policy interventions We evaluate three stylized market and policy configurations representing distinct dynamics and adaptation strategies within the Florida insurance system: (i) private market contraction ("market exit"), (ii) expanded insurance penetration and depopulation of Citizens ("penetration"), and (iii) strengthened building codes and retrofitting ("building code"). Each scenario modifies specific components of the insurance system architecture while holding all other model parameters constant throughout the 10 000 simulated years, enabling isolation of intervention effects on systemic risk metrics.

Private insurer market exit. We model a private insurance market contraction that increases Citizens' market share from 15% (baseline) to 25% of total insured value, corresponding to a 10% shift of exposure from private insurers. Of the exited private exposure, 85% transfers to Citizens and 15% becomes uninsured. Private insurers' surplus levels are reduced in proportion to their exposure contraction, assuming partial retention of fixed capital, while Citizens' surplus requirement scales with market share to the power of 1.2, implying an 84% increase in required surplus for a 66.7% increase in exposure. Gross wind and flood losses remain unchanged; only the pre-event allocation of exposure and capital across entities is modified. The intervention therefore redistributes financial burden without altering physical damages, increasing concentration risk within Citizens and reducing aggregate private capital buffers.

Insurance penetration increase. We model an expansion of insurance coverage and depopulation of Citizens. Wind insurance penetration increases from 40% to 60% of insurable value, and flood insurance penetration from 11% to 30% of insurable value. Flood penetration increases are implemented using county-level FEMA data distinguishing SFHA and non-SFHA areas (65). Baseline penetration rates of approximately 35% within SFHAs and 5% outside SFHAs are scaled by factors of 1.2 and 3.0, respectively, yielding an overall statewide increase from 11% to 30%. Coastal counties receive 1.5$\times$ larger proportional increases than inland counties. NFIP policy counts, coverage amounts, and premium volumes are adjusted proportionally. Concurrently, Citizens' market share decreases from 15% to 8% through active policy transfers to private insurers and higher proportional expansion of private market exposure. Insurer surplus levels scale proportionally with exposure growth. Gross wind and flood losses are unchanged; however, the insured fraction of losses increases and the uninsured household burden decreases. This intervention expands the premium base and shifts loss absorption toward the private market, while reducing Citizens' exposure.

Building code improvement. We model structural loss reduction through enhanced building standards and retrofitting that reduce wind-related losses by 30% and flood-related losses by 25% relative to baseline vulnerability. Loss reductions are applied to wind and flood loss estimates before allocation into insured and uninsured components. Exposure values and insurer capital levels remain unchanged. Unlike the previous two interventions, this scenario reduces total losses rather than reallocating them.

Building code-climate offset analysis We conduct a sensitivity analysis to determine the level of building code improvement required to offset projected mid-century climate change impacts (SSP2-4.5, 2041-2060) and maintain systemic risk levels that exist in the current climate. Using the same Future climate scenarios approach described above, we simulate historical (1995-2014) and future (2041-2060) conditions with 10 000 synthetic years per model. For the future period, we evaluate 13 building code levels representing combined wind and flood loss reductions ranging from 0% to 95%, with wind and flood reductions applied in a fixed 3:2 ratio.

For each GCM and building code level, we compute the climate delta as the difference between the mean of metric M across 10 000 future-period simulated years (with the building-code-induced loss reduction applied) and the mean across the corresponding GCM historical reference period. Ensemble median and 10th-90th percentile deltas across the five GCMs are added to the ERA5 baseline.

Data availability

Data used in this study are available from the sources cited in the Methods section. Data from S&P Capital IQ require a commercial license and are not publicly accessible.

The synthetic TC data from the MIT model are proprietary and owned by WindRiskTech L.L.C., a company that provides hurricane risk assessments to clients worldwide. Due to proprietary restrictions, these datasets are not publicly archived. However, researchers interested in accessing the data for scientific purposes can contact WindRiskTech L.L.C. at info@windrisktech.com, subject to a non-redistribution agreement.

Code availability

For this study, we used the Python (version 3.11+) version of CLIMADA, release v6.1.0-dev (82). Source code is openly and freely available under the terms of the GNU General Public License Version 3 (73).

Code to reproduce the results of this paper is available at a GitHub repository (83) with the identifier 10.5281/zenodo.19361128.

References

1. NOAA National Centers for Environmental Information, 2025: U.S. billion-dollar weather and climate disasters. NOAA National Centers for Environmental Information, doi:10.25921/stkw-7w73.
2. Swiss Re Institute, 2018: Sigma No 1/2018: Natural catastrophes and man-made disasters in 2017: A year of record-breaking losses.
3. Seneviratne, S. I., M. G. Donat, A. J. Pitman, R. Knutti, L. J. Wilcox, and X. Zhang, 2021: Weather and climate extreme events in a changing climate. *Climate Change 2021: The Physical Science Basis. Contribution of Working Group I to the Sixth Assessment Report of the Intergovernmental Panel on Climate Change*, V. Masson-Delmotte, P. Zhai, A. Pirani, S. L. Connors, C. Péan, S. Berger, N. Caud, Y. Chen, L. Goldfarb, M. I. Gomis, M. Huang, K. Leitzell, E. Lonnoy, J. B. R. Matthews, T. K. Maycock, T. Waterfield, O. Yelekçi, R. Yu, and B. Zhou, Eds., Cambridge University Press, Cambridge, United Kingdom and New York, NY, USA, 1513–1766, doi:10.1017/9781009157896.014.
4. Zscheischler, J., S. Westra, B. J. Van Den Hurk, S. I. Seneviratne, P. J. Ward, A. Pitman, A. Aghakouchak, D. N. Bresch, M. Leonard, T. Wahl, and X. Zhang, 2018: Future climate risk from compound events. *Nature Climate Change*, **8 (6)**, 469–477, doi:10.1038/s41558-018-0156-3.
5. Kousky, C., 2019: The Role of Natural Disaster Insurance in Recovery and Risk Reduction. *Annual Review of Resource Economics*, **11**, 399–418, doi:10.1146/annurev-resource-100518-094028.
6. Gallagher, J., and D. Hartley, 2017: Household Finance after a Natural Disaster: The Case of Hurricane Katrina. *American Economic Journal: Economic Policy*, **9 (3)**, 199–228, doi:10.1257/pol.20140273.
7. Kunreuther, H., and M. Useem, Eds., 2010: *Learning from Catastrophes: Strategies for Reaction and Response*. Pearson P T R, Upper Saddle River, N.J.
8. Jarzabkowski, P., K. Chalkias, E. Cacciatori, and R. Bednarek, 2023: *Disaster Insurance Reimagined: Protection in a Time of Increasing Risk*. 1st ed., Oxford University PressOxford, doi:10.1093/oso/9780192865168.001.0001.
9. Kousky, C., G. Treuer, and K. J. Mach, 2024: Insurance and climate risks: Policy lessons from three bounding scenarios. *Proceedings of the National Academy of Sciences*, **121 (48)**, e2317875 121, doi:10.1073/pnas.2317875121.
10. Cummins, J. D., and M. A. Weiss, 2014: Systemic Risk and The U.S. Insurance Sector. *Journal of Risk and Insurance*, **81 (3)**, 489–528, doi:10.1111/jori.12039.
11. Jung, H., R. F. Engle, S. Ge, and X. Zeng, 2023: Physical climate risk factors and an application to measuring insurers' climate risk exposure. Staff Report 1066, Federal Reserve Bank of New York.
12. Boomhower, J., M. Fowlie, J. Gellman, and A. Plantinga, 2024: How Are Insurance Markets Adapting to Climate Change? Risk Classification and Pricing in the Market for Homeowners Insurance, doi:10.3386/w32625, 32625.
13. Oh, S. S., I. Sen, and A.-M. Tenekedjieva, 2026: Pricing of Climate Risk Insurance: Regulation and Cross-Subsidies. *The Journal of Finance*, **81 (3)**, 1161–1215, doi:10.1111/jofi.70029.
14. California Department of Insurance, 2024: 2024 annual report of the insurance commissioner. Tech. rep., California Department of Insurance, Sacramento, CA, USA.

15. Sastry, P., I. Sen, and A.-M. Tenekedjieva, 2023: When Insurers Exit: Climate Losses, Fragile Insurers, and Mortgage Markets, doi:10.2139/ssrn.4674279, 4674279.

16. Kousky, C., and L. Medders, 2024: The evolution of florida's public-private approach to property insurance. Report, Florida Policy Project.

17. Hemmati, M., I. P. Gray, and S. G. Bowen, 2025: The growing void in the U.S. homeowners insurance market: Who should bear the rising cost of climate change? *npj Climate Action*, **4 (1)**, 1–7, doi:10.1038/s44168-025-00231-8.

18. Ben-Shahar, O., and K. D. Logue, 2016: The Perverse Effects of Subsidized Weather Insurance.

19. Kousky, C., and H. Kunreuther, 2014: Addressing Affordability in the National Flood Insurance Program. *Journal of Extreme Events*, **01 (01)**, 1450 001, doi:10.1142/S2345737614500018.

20. Burby, R. J., 2006: Hurricane Katrina and the Paradoxes of Government Disaster Policy: Bringing About Wise Governmental Decisions for Hazardous Areas. *The ANNALS of the American Academy of Political and Social Science*, **604 (1)**, 171–191, doi:10.1177/0002716205284676.

21. Peralta, A., and J. B. Scott, 2024: Does the National Flood Insurance Program Drive Migration to Higher Risk Areas? *Journal of the Association of Environmental and Resource Economists*, **11 (2)**, 287–318, doi:10.1086/726155.

22. Basel Committee on Banking Supervision, 2011: *Basel III: A Global Regulatory Framework for More Resilient Banks and Banking Systems*. December 2010 (rev. june 2011) ed., Basel Bank for International Settlements 2011.

23. International Monetary Fund (IMF), 2012: Macrofinancial stress testing—principles and practices. Tech. rep., International Monetary Fund.

24. Board of Governors of the Federal Reserve System, 2022: Stress tests and capital planning. https://www.federalreserve.gov/supervisionreg/stress-tests-capital-planning.htm, Accessed on 2026-03-31.

25. Battiston, S., A. Mandel, I. Monasterolo, F. Schütze, and G. Visentin, 2017: A climate stress-test of the financial system. *Nature Climate Change*, **7 (4)**, 283–288, doi:10.1038/nclimate3255.

26. Network for Greening the Financial System (NGFS), 2024: NGFS climate scenarios for central banks and supervisors—phase V. Tech. rep., Network for Greening the Financial System (NGFS).

27. Dunz, N., T. Emambakhsh, T. Hennig, M. Kaijser, C. Kouratzoglou, and C. Salleo, 2021: ECB's Economy-Wide Climate Stress Test. *SSRN Electronic Journal*, doi:10.2139/ssrn.3929178.

28. European Central Bank, 2022: 2022 climate risk stress test. Tech. rep., European Central Bank, Banking Supervision.

29. Bank of England, 2022: Results of the 2021 climate biennial exploratory scenario (CBES). Tech. rep., Bank of England.

30. Board of Governors of the Federal Reserve System, 2024: Pilot climate scenario analysis exercise: Summary of participants' risk-management practices and estimates. Tech. rep., Board of Governors of the Federal Reserve System.

31. Swiss Re Institute, 2024: Sigma 1/2024: Natural catastrophes in 2023: Gearing up for today's and tomorrow's weather risks.

32. Task Force on Climate-related Financial Disclosures, 2017: Final report: Recommendations of the task force on climate-related financial disclosures. Technical report, Financial Stability Board.

33. National Association of Insurance Commissioners (NAIC), 2026: NAIC climate risk disclosure survey. https://www.insurance.ca.gov/0250-insurers/0300-insurers/0100-applications/ClimateSurvey/index.cfm, Accessed on 2026-03-31.

34. European Insurance and Occupational Pensions Authority (EIOPA), 2022: Methodological principles of insurance stress testing—climate change component. Tech. rep., European Insurance and Occupational Pensions Authority (EIOPA).

35. Wattin Håkansson, V., S. Meiler, S. Hülsen, L. Villiger, M. Bossut, J. W. McCaughey, C. M. Kropf, and D. N. Bresch, 2025: Beyond single company climate risk disclosure: Event-based physical risk reporting. *Environmental Research: Climate*, **4 (3)**, 035 014, doi:10.1088/2752-5295/adf912.

36. Abrahams, D., and T. Robustelli, 2025: Climate Change, Housing, and Homeowners Insurance in Florida: Lessons for California. http://newamerica.org/future-land-housing/briefs/insurance-in-florida-lessons-for-california/, Accessed on 2026-01-28.

37. Knapp, K. R., M. C. Kruk, D. H. Levinson, H. J. Diamond, and C. J. Neumann, 2010: The International Best Track Archive for Climate Stewardship (IBTrACS). *Bulletin of the American Meteorological Society*, **91 (3)**, 363–376, doi:10.1175/2009BAMS2755.1.

38. Emanuel, K., S. Ravela, E. Vivant, and C. Risi, 2006: A Statistical Deterministic Approach to Hurricane Risk Assessment. *Bulletin of the American Meteorological Society*, **87 (3)**, S1–S5, doi:10.1175/bams-87-3-emanuel.

39. Emanuel, K., R. Sundararajan, and J. Williams, 2008: Hurricanes and global warming: Results from downscaling IPCC AR4 simulations. *Bulletin of the American Meteorological Society*, **89 (3)**, 347–367, doi:10.1175/BAMS-89-3-347.

40. Citizens Property Insurance Corporation, 2024: Policies in force. https://www.citizensfla.com/policies-in-force, Accessed on 2026-03-31.

41. Federal Emergency Management Agency (FEMA), 2024: FIMA NFIP redacted policies (v2). U.S. Department of Homeland

Security, https://www.fema.gov/openfema-data-page/fima-nfip-redacted-policies-v2, Accessed on 2026-03-19.

42. State Board of Administration of Florida, and Florida Hurricane Catastrophe Fund, 2023: Florida hurricane catastrophe fund: 2023 annual report. Tech. rep., State Board of Administration of Florida, Tallahassee, FL.

43. Florida Hurricane Catastrophe Fund, 2024: Florida hurricane catastrophe fund 2024 annual report. State Board of Administration of Florida, Accessed on 2026-03-19.

44. Artemis.bm, 2024: Catastrophe bond and insurance-linked securities deal directory. https://www.artemis.bm/deal-directory/, Accessed on 2026-03-31.

45. Congressional Research Service, 2025: National flood insurance program borrowing authority. https://www.congress.gov/crs_external_products/IN/PDF/IN10784/IN10784.43.pdf, Accessed on 2026-03-31.

46. State of Florida, 2024: Florida statutes. § 215.555 (Florida Hurricane Catastrophe Fund); § 627.351(6) (Citizens Property Insurance Corporation); § 631.57 (Florida Insurance Guaranty Association).

47. Florida Insurance Guaranty Association, 2026: Assessments. https://figafacts.com/assessments/.

48. Citizens Property Insurance Corporation, 2026: Assessments.

49. Muller, J., K. Mooney, S. G. Bowen, P. J. Klotzbach, T. Martin, T. J. Philp, B. Dhruvkumar, R. S. Dixon, and S. B. Girimurugan, 2025: Normalized Hurricane Damage in the United States: 1900–2022. *Bulletin of the American Meteorological Society*, **106 (1)**, E51–E67, doi:10.1175/BAMS-D-23-0280.1.

50. Wolf, D., and K. Takeuchi, 2025: Are Building Codes an Effective Adaptation to Wind Risk? Evidence from Remotely Detected Blue Tarps.

51. Insurance Institute for Business & Home Safety, 2025: 2025 FORTIFIED home standards. https://fortifiedhome.org/wp-content/uploads/2025-FORTIFIED-Home-Standard.pdf, Accessed on 2026-02-19.

52. The Florida Senate, 2011: Citizens property insurance corporation. Issue Brief 2012-226, The Florida Senate, Committee on Banking and Insurance.

53. Florida Legislature, 2006: Senate bill 1980 (2006): Property and casualty insurance. Chapter 2006-12, Laws of Florida.

54. Laeven, L., and F. Valencia, 2020: Systemic banking crises database II. *IMF Economic Review*, **68 (2)**, 307–361, doi:10.1057/s41308-020-00107-3.

55. U.S. Bureau of Economic Analysis, 2026: Gross Domestic Product: All Industry Total in Florida [FLNGSP]. url https://fred.stlouisfed.org/series/FLNGSP, retrieved from FRED, Federal Reserve Bank of St. Louis, Accessed on 2026-06-09.

56. Alabama Department of Insurance and Center for Risk and Insurance Research, 2025: Performance of IBHS FORTIFIED HomeTM construction in hurricane sally. https://aldoi.gov/pdf/news/performanceibhsfortifiedhomeconstructionhurricanesally.pdf, Accessed on 2026-02-19.

57. Meiler, S., A. Ciullo, C. M. Kropf, K. Emanuel, and D. N. Bresch, 2023: Uncertainties and sensitivities in the quantification of future tropical cyclone risk. *Communications Earth & Environment*, **4 (1)**, 1–10, doi:10.1038/s43247-023-00998-w.

58. Vecchi, G. A., C. Landsea, W. Zhang, G. Villarini, and T. Knutson, 2021: Changes in Atlantic major hurricane frequency since the late-19th century. *Nature Communications*, **12**, 4054, doi:10.1038/s41467-021-24268-5.

59. Emanuel, K., 2021: Atlantic tropical cyclones downscaled from climate reanalyses show increasing activity over past 150 years. *Nature Communications*, **12 (1)**, 7027, doi:10.1038/s41467-021-27364-8.

60. Abatzoglou, J. T., and A. P. Williams, 2016: Impact of anthropogenic climate change on wildfire across western US forests. *Proceedings of the National Academy of Sciences*, **113 (42)**, 11 770–11 775, doi:10.1073/pnas.1607171113.

61. Mishra, A., A. Arun, E. Kodra, E. Smull, O. Woolcock, T. Doe, J. Marlowe, and A. R. Ganguly, 2026: Physical climate risk creates challenges and opportunities in US municipal finance. *Nature Cities*, **3 (1)**, 11–21, doi:10.1038/s44284-025-00365-0.

62. Amornsiripanitch, N., S. Biswas, J. Orellana-Li, and D. Zink, 2025: Measuring flood underinsurance in the USA. *Nature Climate Change*, 1–7, doi:10.1038/s41558-025-02396-w.

63. Florida Office of Insurance Regulation, 2024: Quarterly Residential Market Share Reports. https://floir.gov/tools-and-data/residential-market-share-reports, Accessed on 2026-03-19.

64. , 2017: Office of insurance regulation v. state farm florida insurance co., 226 so. 3d 853 (fla. 1st DCA 2017). Florida First District Court of Appeal.

65. Federal Emergency Management Agency (FEMA), 2025: OpenFEMA dataset: NFIP residential penetration rates – v1. U.S. Department of Homeland Security, https://www.fema.gov/openfema-data-page/nfip-residential-penetration-rates-v1, Accessed on 2026-03-19.

66. Citizens Property Insurance Corporation, 2024: Annual statement of the citizens property insurance corporation for the year ended december 31, 2024. Tech. rep., Citizens Property Insurance Corporation, Tallahassee, FL.

67. Hersbach, H., B. Bell, P. Berrisford, S. Hirahara, A. Horányi, J. Muñoz-Sabater, J. Nicolas, C. Peubey, R. Radu, D. Schepers, A. Simmons, C. Soci, S. Abdalla, X. Abellan, G. Balsamo, P. Bechtold, G. Biavati, J. Bidlot, M. Bonavita, G. De Chiara,

P. Dahlgren, D. Dee, M. Diamantakis, R. Dragani, J. Flemming, R. Forbes, M. Fuentes, A. Geer, L. Haimberger, S. Healy, R. J. Hogan, E. Hólm, M. Janisková, S. Keeley, P. Laloyaux, P. Lopez, C. Lupu, G. Radnoti, P. de Rosnay, I. Rozum, F. Vamborg, S. Villaume, and J.-N. Thépaut, 2020: The ERA5 global reanalysis. *Quarterly Journal of the Royal Meteorological Society*, **146 (730)**, 1999–2049, doi:10.1002/qj.3803.

68. Swart, N. C., J. N. S. Cole, V. V. Kharin, M. Lazare, J. F. Scinocca, N. P. Gillett, J. Anstey, V. Arora, J. R. Christian, S. Hanna, Y. Jiao, W. G. Lee, F. Majaess, O. A. Saenko, C. Seiler, C. Seinen, A. Shao, M. Sigmond, L. Solheim, K. von Salzen, D. Yang, and B. Winter, 2019: The Canadian Earth System Model version 5 (CanESM5.0.3). *Geoscientific Model Development*, **12 (11)**, 4823–4873, doi:10.5194/gmd-12-4823-2019.

69. Voldoire, A., D. Saint-Martin, S. Sénési, B. Decharme, A. Alias, M. Chevallier, J. Colin, J.-F. Guérémy, M. Michou, M.-P. Moine, P. Nabat, R. Roehrig, D. Salas y Mélia, R. Séférian, S. Valcke, I. Beau, S. Belamari, S. Berthet, C. Cassou, J. Cattiaux, J. Deshayes, H. Douville, C. Ethé, L. Franchistéguy, O. Geoffroy, C. Lévy, G. Madec, Y. Meurdesoif, R. Msadek, A. Ribes, E. Sanchez-Gomez, L. Terray, and R. Waldman, 2019: Evaluation of CMIP6 DECK Experiments With CNRM-CM6-1. *Journal of Advances in Modeling Earth Systems*, **11 (7)**, 2177–2213, doi:10.1029/2019MS001683.

70. EC Earth Consortium, 2019: EC-Earth-Consortium EC-Earth3 model output prepared for CMIP6 ScenarioMIP ssp245. Accessed on 2023-02-16, doi:10.22033/ESGF/CMIP6.4880.

71. Hourdin, F., C. Rio, J.-Y. Grandpeix, J.-B. Madeleine, F. Cheruy, N. Rochetin, A. Jam, I. Musat, A. Idelkadi, L. Fairhead, M.-A. Foujols, L. Mellul, A.-K. Traore, J.-L. Dufresne, O. Boucher, M.-P. Lefebvre, E. Millour, E. Vignon, J. Jouhaud, F. B. Diallo, F. Lott, G. Gastineau, A. Caubel, Y. Meurdesoif, and J. Ghattas, 2020: LMDZ6A: The Atmospheric Component of the IPSL Climate Model With Improved and Better Tuned Physics. *Journal of Advances in Modeling Earth Systems*, **12 (7)**, e2019MS001 892, doi:10.1029/2019MS001892.

72. Tatebe, H., T. Ogura, T. Nitta, Y. Komuro, K. Ogochi, T. Takemura, K. Sudo, M. Sekiguchi, M. Abe, F. Saito, M. Chikira, S. Watanabe, M. Mori, N. Hirota, Y. Kawatani, T. Mochizuki, K. Yoshimura, K. Takata, R. O'ishi, D. Yamazaki, T. Suzuki, M. Kurogi, T. Kataoka, M. Watanabe, and M. Kimoto, 2019: Description and basic evaluation of simulated mean state, internal variability, and climate sensitivity in MIROC6. *Geoscientific Model Development*, **12 (7)**, 2727–2765, doi:10.5194/gmd-12-2727-2019.

73. Aznar-Siguan, G., and D. N. Bresch, 2019: CLIMADA v1: A global weather and climate risk assessment platform. *Geoscientific Model Development*, **12 (7)**, 3085–3097, doi:10.5194/gmd-12-3085-2019.

74. IPCC, 2012: *Managing the Risks of Extreme Events and Disasters to Advance Climate Change Adaptation: A Special Report of Working Groups I and II of the Intergovernmental Panel on Climate Change*. Cambridge University Press, Cambridge, UK and New York, NY, USA, doi:10.1017/CBO9781139177245.

75. Holland, G., 2008: A revised hurricane pressure-wind model. *Monthly Weather Review*, **136 (9)**, 3432–3445, doi:10.1175/2008MWR2395.1.

76. Eberenz, S., D. Stocker, T. Röösli, and D. N. Bresch, 2020: Asset exposure data for global physical risk assessment. *Earth System Science Data*, **12 (2)**, 817–833, doi:10.5194/essd-12-817-2020.

77. Eberenz, S., S. Lüthi, and D. N. Bresch, 2021: Regional tropical cyclone impact functions for globally consistent risk assessments. *Natural Hazards and Earth System Sciences*, **21 (1)**, 393–415, doi:10.5194/nhess-21-393-2021.

78. Liu, J., C. B. Steinmann, D. N. Bresch, S. Meiler, U. Lohmann, and B. Hohermuth, 2026: Recalibrating Risk: A simplified model for North Atlantic hurricanes in a warming climate. *Journal of Catastrophe Risk and Resilience*, **04 (03)**, doi:10.63024/zd46-e3zf.

79. Gori, A., N. Lin, D. Chavas, M. Oppenheimer, and S. Xian, 2025: Sensitivity of tropical cyclone risk across the US to changes in storm climatology and socioeconomic growth. *Environmental Research Letters*, **20 (6)**, 064 050, doi:10.1088/1748-9326/add60d.

80. Gori, A., 2025: Tropical Cyclone Synthetic Hazard and Damage Simulations. DesignSafe-CI, Accessed on 2026-02-12, doi:10.17603/ds2-0jkm-h487.

81. Camargo, S. J., 2013: Global and regional aspects of tropical cyclone activity in the CMIP5 models. *Journal of Climate*, **26 (24)**, 9880–9902, doi:10.1175/JCLI-D-12-00549.1.

82. Siguan, G. A., D. N. Bresch, S. Eberenz, J. Hartman, M. Perus, T. Röösli, D. Stocker, V. Bozzini, C. B. Steinmann, E. Mühlhofer, R. Bungerer, I. J. Sauer, S. Lüthi, P. M. M. Kam, S. Meiler, A. Ciullo, T. Vogt, B. P. Guillod, C. M. Kropf, E. Schmid, C. Fairless, J. Wüthrich, Z. Stalhandske, Y. Yu, L. Riedel, R. Portmann, N. Colombi, L. Villiger, T. Schmid, L. Severino, S. Juhel, V. Gebhart, and D. Araya, 2025: CLIMADA Core Python Package. Zenodo, Accessed on 2026-03-23, doi:10.5281/zenodo.17233409.

83. Meiler, S., 2026: Simonameiler/systemic_insurance_risk_fl_pub: V1.0.0. Zenodo, Accessed on 2026-03-31, doi:10.5281/zenodo.19361128.

84. Smith, A. B., and R. W. Katz, 2013: US billion-dollar weather and climate disasters: Data sources, trends, accuracy and biases. *Natural Hazards*, **67 (2)**, 387–410, doi:10.1007/s11069-013-0566-5.

85. Smith, A. B., and J. L. Matthews, 2015: Quantifying uncertainty and variable sensitivity within the US billion-dollar weather and climate disaster cost estimates. *Natural Hazards*, **77 (3)**, 1829–1851, doi:10.1007/s11069-015-1678-x.
86. Florida Office of Insurance Regulation, 2026: Catastrophe Reporting. https://floir.gov/tools-and-data/catastrophe-reporting, Accessed on 2026-03-19.
87. National Flood Insurance Program, 2026: Historical NFIP Claims Information and Trends. https://www.floodsmart.gov/historical-nfip-claims-information-and-trends, Accessed on 2026-03-19.
88. Federal Emergency Management Agency (FEMA), 2026: Disaster Declarations Summaries - v2. U.S. Department of Homeland Security, https://www.fema.gov/openfema-data-page/disaster-declarations-summaries-v2, Accessed on 2026-03-19.
89. US Bureau of Labor Statistics, 2026: Consumer Price Index for All Urban Consumers (CPI-U). https://data.bls.gov/PDQWeb/cu, Accessed on 2026-03-19.

Acknowledgements

Funding

SM acknowledges support from the Swiss National Science Foundation Postdoc.Mobility Fellowship (P500PN_222189) and from the Stanford Urban Resilience Initiative. NSD acknowledges support from Stanford University.

The development of the risk propagation model underlying this study was initiated in collaboration with the Insurance Policy Advisory Committee (IPAC) of the U.S. Federal Reserve System, for which Simona Meiler developed an initial flow-of-risk modeling approach. We thank members of the IPAC Property Insurance Working Group for valuable discussions and insights that informed the conceptual design of the model. The analysis presented here represents independent academic work and does not reflect the views of the Federal Reserve System or its committees.

Author contributions statement

Conceptualization: SM, SIJ
Methodology: SM
Visualization: SM
Datasets: SM, SIJ, KE
Writing - original draft: SM
Writing - review & editing: SM, SIJ, KE, NSD, JWB

Competing interests

All authors (SM, SIJ, KE, NSD, JWB) declare no competing interests. Kerry Emanuel is on the board of Trusted Resource Underwriters, which insures homeowners in Florida.

Supplementary Information for article "Stress testing insurance market stability under climate risk"

Supplementary Methods

Estimation of insured loss fractions for tropical cyclone events

To estimate the fraction of economic losses covered by insurance for tropical cyclone events, we reconstruct empirical relationships between insured and total economic losses using Florida-specific data. Our approach follows the methodology of the U.S. Billion-Dollar Weather and Climate Disaster Database (84, 85), in which total economic losses are inferred from insured losses, National Flood Insurance Program (NFIP) payouts, and federal disaster assistance.

Total economic losses are estimated as:

$$L_{\text{econ}} = 2 \cdot L_{\text{insured}} + L_{\text{NFIP}} + L_{\text{FDA}}, \tag{20}$$

where L_{insured} denotes insured losses reported by the Florida Office of Insurance Regulation (OIR), L_{NFIP} represents NFIP payouts, and L_{FDA} denotes federal disaster assistance. Following (84), the factor of two applied to insured losses accounts for uninsured private losses.

Because the treatment of federal disaster assistance in economic loss accounting is uncertain, we compute two estimates of economic losses: one including L_{FDA} and one excluding it. The insured fraction is then calculated for both formulations as:

$$f_{\text{insured}} = \frac{L_{\text{insured}}}{L_{\text{econ}}}, \tag{21}$$

and averaged across both estimates.

We compile insured loss data from the Florida OIR for hurricane-related losses (2017–2020 and 2022–2024) (86), complemented by NFIP payout data from FEMA's Floodsmart database (87) and federal disaster assistance from FEMA disaster summaries (88). All monetary values are converted to 2024 USD using the Consumer Price Index (CPI-U) from the U.S. Bureau of Labor Statistics (89).

Estimated insured shares vary substantially across years (table S1), ranging from approximately 10% in low-loss years to nearly 50% in high-loss years. Years with large economic losses (exceeding $25 billion) consistently exhibit insured shares above 40%, indicating that insurance penetration increases with event severity.

Table S1: Insured and estimated economic losses and resulting insured shares for Florida hurricane events (2017–2024). Economic losses are estimated using formulations including and excluding federal disaster assistance (FDA). All values are converted to 2024 USD.

Year	Insured losses	Est econ loss (incl. FDA)	f_{insured} (incl.)	Est econ loss (excl. FDA)	f_{insured} (excl.)
2017	28,159,458,046	60,750,223,673	46.35%	57,644,860,280	48.85%
2018	11,472,501,417	26,081,530,262	43.99%	23,251,364,093	49.34%
2019	23,342,615	198,468,914	11.76%	80,793,892	28.89%
2020	699,057,474	2,041,794,621	34.24%	1,783,712,209	39.19%
2021	—	—	—	—	—
2022	23,914,182,689	56,175,193,964	42.57%	53,075,926,756	45.06%
2023	318,470,377	1,754,055,340	18.16%	1,315,565,662	24.21%
2024	7,466,073,319	25,060,543,556	29.79%	22,700,454,161	32.89%
Mean			32.41%		38.35%
Median			34.24%		39.19%
High-loss mean (> $25B)			40.68%		44.03%

Averaging across all years, estimation approaches, and subsets of high-loss years yields an overall mean insured share of 38.9%. Given that the stress-test scenarios considered in this study focus on severe hurricane events and loss years, we adopt a representative insured fraction of 40% for wind-related losses. To account for uncertainty, this fraction is implemented as a Beta distribution centered at 0.4 (Beta(4,6)), reflecting variability around the empirical mean while emphasizing higher insured shares in large-loss events.

Table S2: Definitions of systemic risk metrics used in the main text and Supplementary Information.

Metric	Unit	Definition	Used in
Loss decomposition			
Total loss	USD	Aggregate economic tropical cyclone loss before redistribution across insurance and public backstop layers.	Table 1, Tables S2–S3, Figs. 2, 6
Insured wind – private	USD	Wind-related losses allocated to private admitted-market insurers in the initial risk-absorption layer.	Table 1, Tables S2–S3, Fig. 2
Citizens wind	USD	Wind-related losses allocated to Citizens in the initial risk-absorption layer.	Table 1, Tables S2–S3, Fig. 2
Insured flood – NFIP	USD	Flood-related losses allocated to the NFIP.	Table 1, Tables S2–S3, Fig. 2
Un/underinsured wind	USD	Wind-related damages not covered by private insurance or Citizens because of un- or underinsurance.	Table 1, Tables S2–S3, Fig. 2
Un/underinsured flood	USD	Flood-related damages not covered by the NFIP because of un- or underinsurance.	Table 1, Tables S2–S3, Fig. 2
Household burden	USD	Combined un/underinsured wind and flood losses.	Fig. 2
Insured / uninsured share	%	Share of total loss that is insured or un/underinsured.	Fig. 2
Institutional stress and public burden			
FHCF shortfall	USD	Unrecovered wind losses resulting when the FHCF season-wide payout cap binds.	Table 1, Tables S2–S3, Figs. 2, S2
FIGA residual	USD	Residual deficit remaining after insurer insolvencies are absorbed through the FIGA, subject to its assessment limits.	Table 1, Tables S2–S3, Figs. 2, S2
Citizens deficit	USD	Residual deficit remaining after Citizens' surplus and assessment capacity are exhausted.	Table 1, Tables S2–S3, Figs. 2, S2
NFIP Treasury borrowing	USD	Portion of Florida-attributable NFIP losses financed through borrowing from the U.S. Treasury once NFIP fund balances are insufficient.	Table 1, Tables S2–S3, Figs. 2, S2
Total public burden	USD	The sum of FHCF shortfall, FIGA residual, Citizens deficit, and NFIP Treasury borrowing.	Table 1, Tables S2–S3, Figs. 2, 6
Capital depletion and default outcomes			
Private defaults	#	Number of private insurer entities that become insolvent under a simulated event or season after modeled capital depletion.	Table S2, Figs. 3–4, S2
Largest single-entity deficit	USD	Maximum capital shortfall of any one insurer entity in a simulated event or season.	Table S2, Figs. 3–4, Fig. S2
Stress ratios			
FHCF utilization factor	ratio	Share of the FHCF season-wide statutory payout capacity utilized in a given scenario or simulation. A value of 1 indicates that the cap is fully used.	Table S2
Citizens assessment stress factor	ratio	Citizens' deficit divided by its maximum assessment capacity (Tier 1 + Tier 2). Values above 1 indicate that the funding need exceeds statutory capacity.	Table S2
FIGA stress factor	ratio	Insolvency-related deficit relative to FIGA's effective maximum assessment capacity. Values above 1 indicate exceedance of capacity.	Table S2
NFIP Florida stress factor	ratio	Florida-attributable NFIP claims paid divided by Florida NFIP annual premium volume.	Table S2
Probabilistic exceedance metrics			
Defaults > 10	annual probability (%)	Probability that more than ten private insurers default in a simulated tropical cyclone season.	Figs. 3–5, Table S4
Single deficit $>$ \$1B	annual probability (%)	Probability that the largest single-company deficit exceeds USD 1 billion in a simulated season.	Figs. 3–5, Table S4
FHCF $> 100\%$ cap	annual probability (%)	Probability that modeled FHCF payouts reach or exceed the season-wide statutory cap.	Figs. 3–5, Table S4
FIGA $> 100\%$ capacity	annual probability (%)	Probability that FIGA funding needs exceed its statutory assessment capacity.	Figs. 3–5, Table S4
Citizens $> 100\%$ capacity	annual probability (%)	Probability that Citizens' deficit exceeds its assessment capacity.	Figs. 3–5, Table S4
NFIP $> 200\%$ annual premium	annual probability (%)	Probability that Florida-attributable NFIP losses exceed twice Florida NFIP annual premium income.	Figs. 3–5, Table S4
Public burden $> 1\%$ Florida GDP	annual probability (%)	Probability that total public burden exceeds 1% of Florida's GDP in a simulated season.	Figs. 3–5, Table S4
Public burden $> 10\%$ Florida GDP	annual probability (%)	Probability that total public burden exceeds 10% of Florida's GDP in a simulated season.	Figs. 3–5, Table S4

Table S3: Scenario-based loss decomposition and institutional stress outcomes for Florida hurricane events. Results are reported as mean values across stochastic realizations, with uncertainty ranges in parentheses indicating the 5th–95th percentiles. Metric definitions are provided in table S2. Named storms denote stylized hazard footprints evaluated on 2024 exposure and insurance-market conditions, not reconstructions of the original events or their realized losses.

Metric	Great Miami	Andrew	Lake Okeechobee	Irma	Great Miami then Andrew	Double Great Miami	Double Irma
Loss decomposition							
Total loss (USD)	170.4B (170.4-170.4B)	114.2B (114.2-114.2B)	156.9B (156.9-156.9B)	32.0B (32.0-32.0B)	266.5B (266.5-266.5B)	321.1B (321.1-321.1B)	62.4B (62.4-62.4B)
Insured wind – private (USD)	36.9B (20.2-56.1B)	29.0B (14.0-46.4B)	16.3B (4.3-31.6B)	6.0B (2.8-9.5B)	61.4B (35.6-90.6B)	69.3B (42.7-98.1B)	11.5B (7.4-15.9B)
Citizens wind (USD)	10.3B (4.9-17.1B)	10.3B (4.6-17.7B)	2.6B (0.7-5.1B)	0.5B (0.2-0.7B)	18.8B (9.7-30.0B)	19.4B (10.5-30.5B)	0.9B (0.6-1.2B)
Insured flood – NFIP (USD)	15.0B (4.9-27.7B)	4.9B (0.5-12.9B)	17.0B (10.5-22.4B)	2.6B (1.3-4.0B)	19.8B (9.4-31.9B)	28.1B (16.1-41.4B)	5.2B (3.6-6.7B)
Un/Underinsured wind (USD)	72.2B (42.5-101.3B)	60.5B (37.8-84.5B)	28.3B (7.6-55.4B)	9.7B (4.7-14.9B)	122.9B (84.4-165.0B)	136.7B (96.0-180.5B)	18.7B (12.8-25.5B)
Un/Underinsured flood (USD)	35.9B (11.4-66.8B)	9.4B (0.9-24.7B)	92.6B (57.3-121.9B)	13.3B (6.5-20.1B)	43.7B (20.5-70.7B)	67.7B (38.5-100.1B)	26.1B (18.0-33.8B)
Institutional stress							
Total public burden (USD)	26.1B (15.4-38.8B)	11.7B (4.1-22.3B)	18.4B (16.6-20.9B)	0.2B (0.0-0.8B)	51.0B (28.7-74.0B)	65.4B (42.7-88.3B)	3.1B (2.1-4.0B)
FHCF shortfall (USD)	1.7B (0.0-8.0B)	0.0B (0.0-0.0B)	0.0B (0.0-0.0B)	0.0B (0.0-0.0B)	5.6B (0.0-11.6B)	8.0B (0.0-12.7B)	0.0B (0.0-0.0B)
FIGA residual (USD)	7.0B (3.2-13.4B)	4.2B (1.1-10.0B)	3.3B (0.0-8.8B)	0.1B (0.0-0.7B)	15.8B (6.2-27.7B)	19.1B (8.5-31.1B)	1.3B (0.1-2.8B)
Citizens deficit (USD)	5.8B (3.1-11.4B)	5.2B (1.9-11.9B)	1.6B (0.0-4.0B)	0.0B (0.0-0.0B)	13.2B (4.7-24.1B)	13.6B (5.5-24.7B)	0.0B (0.0-0.3B)
NFIP treasury borrowing (USD)	11.5B (1.4-24.3B)	2.2B (0.0-9.4B)	13.6B (7.1-18.9B)	0.1B (0.0-0.5B)	16.4B (6.0-28.5B)	24.7B (12.7-38.0B)	1.8B (0.2-3.3B)
Capital & default assessment							
Private defaults (#)	18 (15-22)	16 (12-20)	13 (0-18)	5 (0-11)	21 (18-23)	22 (19-24)	12 (8-14)
Largest single-entity deficit (USD)	1.9B (1.1-3.3B)	1.2B (0.4-2.8B)	1.0B (0.0-2.4B)	0.1B (0.0-0.4B)	3.8B (1.6-6.8B)	4.6B (2.2-7.5B)	0.6B (0.2-1.0B)
Stress ratios							
FHCF utilization factor	0.79 (0.20-1.00)	0.74 (0.25-0.93)	0.02 (0.00-0.08)	0.00 (0.00-0.00)	0.98 (0.87-1.00)	0.98 (0.92-1.00)	0.00 (0.00-0.01)
Citizens assessment stress factor	6.46 (3.43-12.64)	5.83 (2.16-13.26)	1.74 (0.00-4.46)	0.00 (0.00-0.00)	14.67 (5.26-26.77)	15.13 (6.07-27.40)	0.06 (0.00-0.29)
FIGA stress factor	0.95 (0.91-0.98)	0.88 (0.74-0.97)	0.77 (0.00-0.97)	0.17 (0.00-0.67)	0.98 (0.95-0.99)	0.98 (0.97-0.99)	0.70 (0.23-0.89)
NFIP Florida stress factor	10.73 (3.49-19.86)	3.54 (0.35-9.23)	12.19 (7.56-16.02)	1.90 (0.95-2.85)	14.20 (6.74-22.89)	20.13 (11.54-29.68)	3.71 (2.58-4.79)

Table S4: Loss decomposition and public institutional burden across climate and policy scenarios. Values show expected annual losses and institutional burdens under present-day baseline conditions, future climate scenarios (2050 and 2100 under SSP2-4.5 and SSP5-8.5), and illustrative market and policy interventions evaluated under present-day climate forcing. Values are reported as means in billion USD with uncertainty ranges (10th–90th percentile) in parentheses.

Metric (USD B)	Baseline	2050 SSP2-4.5	2050 SSP5-8.5	2100 SSP2-4.5	2100 SSP5-8.5	Market Exit	Insurance Penetration	Building Codes
Loss decomposition								
Total loss	19.3 (0.0–37.8)	31.5 (15.3–45.5)	34.9 (17.6–55.6)	41.9 (18.3–50.0)	59.2 (22.2–104.2)	19.3 (0.0–37.8)	19.3 (0.0–37.9)	19.3 (0.0–38.0)
Insured wind – private	5.5 (0.0–11.6)	13.9 (6.7–19.9)	15.4 (7.8–24.3)	18.5 (8.1–22.1)	26.2 (9.8–46.0)	4.7 (0.0–9.8)	8.1 (0.0–17.3)	3.8 (0.0–8.1)
Citizens wind	1.1 (0.0–1.8)	2.6 (1.3–3.8)	2.9 (1.5–4.6)	3.4 (1.5–4.1)	4.7 (1.8–8.6)	1.9 (0.0–3.5)	1.7 (0.0–2.8)	0.8 (0.0–1.2)
Insured flood – NFIP	0.6 (0.0–0.9)	1.5 (0.8–2.3)	1.7 (0.8–2.7)	1.9 (0.9–2.3)	2.7 (1.0–5.0)	0.6 (0.0–0.9)	1.7 (0.0–2.4)	0.5 (0.0–0.7)
Un/underinsured wind	9.7 (0.0–19.8)	7.3 (3.6–10.8)	8.3 (4.1–13.1)	9.9 (4.3–11.8)	14.0 (5.2–24.5)	9.7 (0.0–19.8)	6.5 (0.0–13.4)	11.7 (0.0–23.8)
Un/underinsured flood	2.4 (0.0–3.9)	6.2 (2.9–8.8)	6.6 (3.4–10.8)	8.2 (3.5–9.6)	11.5 (4.3–20.1)	2.4 (0.0–3.9)	1.3 (0.0–2.0)	2.6 (0.0–4.1)
Institutional stress								
Total public burden	2.7 (0.0–1.7)	7.1 (3.3–11.0)	7.8 (4.0–13.9)	9.6 (4.1–12.3)	14.9 (5.1–29.7)	3.1 (0.0–2.7)	5.1 (0.0–2.5)	1.6 (0.0–0.5)
FHCF shortfall	0.3 (0.0–0.0)	1.0 (0.4–1.6)	1.1 (0.6–2.1)	1.5 (0.6–2.0)	2.5 (0.8–5.1)	0.4 (0.0–0.0)	0.7 (0.0–0.0)	0.2 (0.0–0.0)
FIGA residual	1.3 (0.0–1.0)	3.4 (1.6–5.2)	3.8 (1.9–6.6)	4.7 (2.0–6.0)	7.3 (2.5–14.3)	1.1 (0.0–0.7)	2.0 (0.0–1.0)	0.8 (0.0–0.3)
Citizens deficit	0.7 (0.0–0.7)	1.8 (0.9–2.8)	2.0 (1.0–3.4)	2.4 (1.0–3.0)	3.5 (1.3–6.9)	1.3 (0.0–2.1)	1.2 (0.0–1.6)	0.5 (0.0–0.2)
NFIP Treasury borrowing	0.3 (0.0–0.0)	0.8 (0.4–1.4)	0.9 (0.5–1.7)	1.0 (0.4–1.4)	1.7 (0.6–3.4)	0.3 (0.0–0.0)	1.2 (0.0–0.0)	0.2 (0.0–0.0)

Table S5: Probabilistic exceedance of systemic insurance stress thresholds across climate and policy scenarios. Annual exceedance probabilities (percent) of systemic stress thresholds for private insurers, public and quasi-public institutions, and aggregate fiscal impact, estimated from 10000 simulated tropical cyclone seasons. Results are shown for present-day conditions, mid-century (2050) and end-of-century (2100) climate scenarios under SSP2-4.5 and SSP5-8.5, as well as illustrative market and policy interventions evaluated under present-day climate forcing. Values denote mean probabilities, with uncertainty ranges (10th–90th percentile) in parentheses.

Metric (%)	Baseline	2050 SSP2-4.5	2050 SSP5-8.5	2100 SSP2-4.5	2100 SSP5-8.5	Market Exit	Insurance Penetration	Building Codes
Defaults > 10	11.4 (10.9-11.8)	17.7 (12.6-20.6)	18.8 (13.1-22.2)	20.2 (13.5-21.3)	22.7 (14.6-27.3)	10.3 (9.9-10.7)	9.7 (9.3-10.0)	9.2 (8.8-9.6)
Single Deficit > $1B	7.2 (6.9-7.5)	11.5 (7.9-14.2)	12.2 (8.6-15.9)	13.5 (8.8-15.1)	16.6 (9.9-22.8)	6.5 (6.2-6.8)	8.2 (7.9-8.6)	5.6 (5.3-5.9)
FHCF > 100% Cap	0.8 (0.7-0.9)	0.9 (0.7-1.1)	1.0 (0.7-1.2)	1.0 (0.7-1.1)	1.2 (0.8-1.6)	0.7 (0.6-0.8)	1.2 (1.0-1.3)	0.5 (0.4-0.6)
FIGA > 100% Capacity	13.6 (13.2-14.1)	22.1 (15.1-27.5)	23.3 (16.6-30.9)	26.0 (17.0-29.4)	32.3 (19.0-45.3)	12.8 (12.3-13.2)	13.4 (13.0-13.9)	11.5 (11.1-11.9)
Citizens > 100% Capacity	9.5 (9.2-9.9)	15.1 (10.4-18.8)	16.1 (11.2-20.8)	17.3 (11.5-19.4)	21.0 (12.6-29.5)	13.0 (12.6-13.4)	11.8 (11.3-12.2)	7.9 (7.6-8.3)
NFIP > 200% Annual Premium	5.0 (4.8-5.3)	5.9 (4.4-6.9)	6.1 (4.6-7.5)	6.6 (4.7-7.2)	7.7 (5.0-10.0)	5.0 (4.8-5.3)	9.3 (8.9-9.7)	4.0 (3.7-4.2)
Public Burden > 1% FL GDP	3.7 (3.5-3.9)	4.3 (3.2-5.1)	4.5 (3.4-5.5)	4.9 (3.4-5.3)	5.6 (3.7-7.3)	4.3 (4.0-4.5)	5.6 (5.3-5.9)	2.4 (2.2-2.6)
Public Burden > 10% FL GDP	0.1 (0.1-0.2)	0.2 (0.1-0.2)	0.2 (0.1-0.2)	0.2 (0.1-0.2)	0.2 (0.1-0.3)	0.2 (0.1-0.3)	0.7 (0.6-0.8)	0.0 (0.0-0.1)

Sensitivity to the insured wind fraction

The assumed insured wind fraction materially affects systemic-risk outcomes. Table S6 reports model outputs across fixed values of the insured wind fraction f_W from 0.1 to 0.5. Reducing f_W from the baseline 0.4 to 0.1 lowers the mean FIGA residual deficit by 88%, while increasing uninsured and underinsured household wind losses by 50%. Backstop-mechanism outcomes respond more than proportionally to changes in f_W, because a higher insured fraction routes more wind losses through insurer balance sheets, elevating default risk and amplifying downstream FIGA, Citizens, and group-capital shortfalls. Because wind insurance penetration is inferred indirectly and calibrated to approximately 40% in extreme events, the model may overstate coverage in smaller events but aligns with observed take-up rates in the large-loss years that dominate systemic-risk outcomes. The qualitative conclusions, in particular the concentration of stress in FIGA, Citizens, and the NFIP rather than the FHCF, are stable across this range, while the dollar magnitudes scale with f_W.

Table S6: Sensitivity of model outputs to the insured wind loss fraction. Mean values (in $B; insurer defaults reported as counts) for each output metric across five fixed values of the insured wind fraction f. The table also reports the relative change compared to the reference case ($f = 0.4$, the mean of the baseline Beta(4, 6) prior) and the approximate log–log elasticity ε evaluated at $f = 0.4$. Metrics with $\varepsilon \approx 0$ are invariant to the insured fraction by construction; $\varepsilon = 1$ indicates proportional scaling; and $\varepsilon > 1$ indicates amplification through the insurance system.

	Mean value ($B)					Change vs. f=0.4				
Metric	f=0.1	f=0.2	f=0.3	f=0.4	f=0.5	$\Delta_{0.1}$	$\Delta_{0.2}$	$\Delta_{0.3}$	$\Delta_{0.5}$	ε
Loss decomposition										
Wind insured — private	1.36	2.72	4.08	5.44	6.80	-75%	-50%	-25%	+25%	+1.00
Wind insured — Citizens	0.27	0.53	0.80	1.07	1.34	-75%	-50%	-25%	+25%	+1.00
Wind un/underinsured	10.26	9.12	7.98	6.84	5.70	+50%	+33%	+17%	-17%	-0.66
Institutional stress										
FHCF shortfall	0.02	0.10	0.22	0.36	0.50	-95%	-74%	-39%	+39%	+1.60
FIGA residual deficit	0.15	0.46	0.84	1.27	1.72	-88%	-64%	-34%	+36%	+1.40
Citizens residual deficit	0.12	0.29	0.49	0.71	0.94	-84%	-60%	-31%	+32%	+1.28
Capital / defaults										
Insurer defaults (count)	0.8186	1.4122	1.8586	2.1992	2.4831	-63%	-36%	-15%	+13%	+0.57
Largest entity deficit	0.05	0.13	0.22	0.32	0.43	-84%	-59%	-31%	+32%	+1.25

Contributions of hazard and parameter uncertainty

In the probabilistic assessment, outcome variability is driven primarily by differences in synthetic event realizations rather than by parameter sampling. We quantify this with a nested Monte Carlo variance decomposition. We select 300 seasons spanning the full range of the loss distribution, rather than drawn at random, and replay each 50 times with ndependent parameter draws. A one-way ANOVA statistic η^2 then measures the fraction of total variance in each output metric attributable to between-season (hazard) differences. Hazard realization explains $\geq 73\%$ of the variance across all metrics and $\geq 95\%$ for every metric except those linked to flooding; for flood-related metrics, the remaining $\sim$25% parameter contribution arises from the wind/water share Beta prior, which governs how much total damage is routed to the NFIP versus the private wind market (Table S7).

Table S7: Relative contributions of hazard variability and parameter uncertainty to model output variance. Values of η^2 from a one-way ANOVA applied to a nested Monte Carlo design (300 seasons $\times$ 50 independent parameter draws per season), measuring the fraction of total variance attributable to between-season hazard differences versus within-season parameter uncertainty. $\eta^2 \geq 0.95$ for all non-flood metrics indicates that hazard realization dominates; the lower values for flood-linked metrics reflect the wind/water share Beta prior, which controls how much total damage is routed to NFIP versus private wind coverage.

Metric	η^2 (hazard)	$1-\eta^2$ (parameters)
Loss decomposition		
Private insurer wind losses	0.976	0.024
Citizens wind losses	0.964	0.036
NFIP flood (insured)	0.772	0.228
Un/underinsured wind	0.977	0.023
Un/underinsured flood	0.749	0.251
Institutional stress		
FHCF shortfall	0.944	0.056
FIGA residual deficit	0.965	0.035
Citizens residual deficit	0.954	0.046
NFIP Treasury borrowing	0.734	0.266
Defaults		
Insurer defaults (count)	0.990	0.010
Largest entity deficit	0.961	0.039

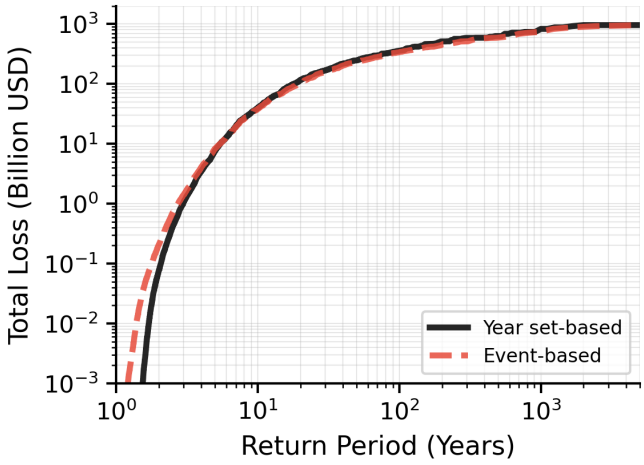

Fig. S1: Return period curves for total tropical cyclone losses in Florida. Event-based losses (red dashed line) and seasonal aggregate losses (solid black line) are shown. Event-based return periods are derived from the empirical exceedance distribution of single events in the historical tropical cyclone event set (8800 events covering 1980–2023; Section Tropical cyclone track data). Seasonal return periods are computed from the empirical exceedance distribution of aggregate losses across simulated 10 000 tropical cyclone years (Section Hazard and loss modeling).

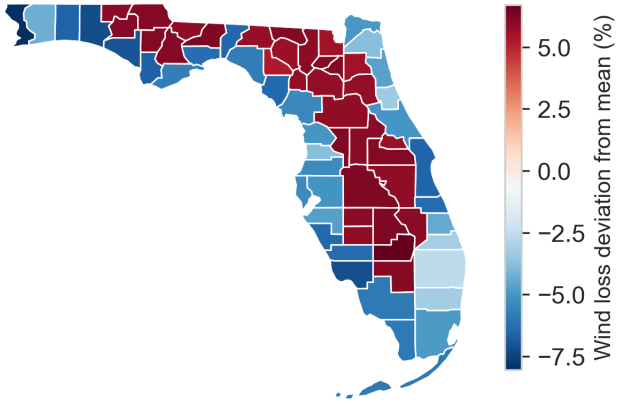

Fig. S2: County-level deviation in wind loss attribution across Florida. Percentage-point deviation of county-specific wind shares from the state-wide mean, derived from the upper 95th percentile of the compound hazard distribution in the synthetic tropical cyclone event set (cf. Methods Wind and flood loss estimation). Positive values indicate wind-dominated counties; negative values indicate relatively stronger flood contributions.

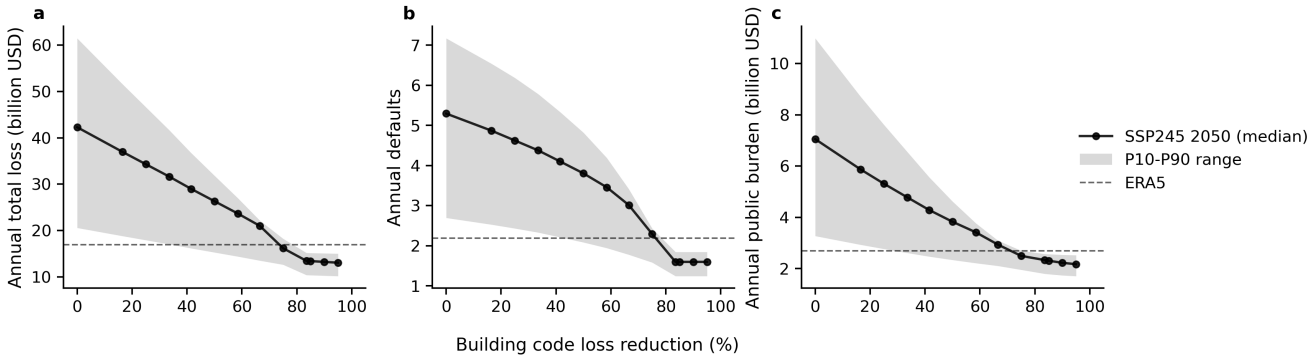

Fig. S3: Sensitivity of systemic insurance outcomes to building code–related loss reductions under future climate conditions. Sensitivity analysis showing the effect of incremental reductions in wind- and flood-related losses resulting from strengthened building codes on systemic risk outcomes under mid-century (2041-2060) SSP2-4.5 climate conditions. Shown are a) annual total loss, b) annual number of private insurer defaults, and c) annual total public burden. Solid lines indicate results for the median climate-induced risk change across the GCM ensemble, shaded bands show the 10th–90th percentile range across GCMs, and dashed lines denote the present-day ERA5 baseline. All quantities represent mean annual outcomes across 10 000 simulated tropical cyclone seasons per climate realization.

Table S8: Ideal data inputs and the publicly available proxies and models used in this study. For each component of the modeling framework, we list the data that a regulator or supervisor with statutory data-collection authority could, in principle, obtain (ideal data input), the public proxy or model adopted here, and the direction in which that choice biases systemic-risk estimates.

Component	Ideal data inputs	Public proxy or model used here	Effect on systemic-risk estimates
Hazard and loss generation			
TC hazard	TC event catalog including wind, rainfall, and storm-surge fields and future sea-level-rise (SLR) projections	Historical (IBTrACS) and synthetic (MIT model) TC events for present and future climate; peak sustained wind as the hazard, with rainfall and surge represented indirectly (see Vulnerability and Wind–flood split)	Omission of SLR underestimates future risk (downward bias); the 1980–2023 baseline may raise losses relative to longer-record industry catalogs (upward bias); remaining choices ambiguous
Asset exposure	Property-level replacement-cost values (TIV) by structure and occupancy	Total asset values from the LitPop method: 2020 GDP disaggregated by nightlight intensity and population at ca. 4 km resolution	Approximates the spatial distribution of value rather than replacement cost; includes non-residential assets, partly absorbed by the empirically calibrated insured fraction (Methods) (ambiguous)
Vulnerability	Residential, structure-specific damage functions	Regionally calibrated USA impact function, wind-parameterized, fit to total losses	Embeds non-residential damage and the average surge/rainfall contribution (ambiguous)
Wind–flood split	Event-level claims by peril (wind, surge, rainfall)	County-level multi-hazard regression (Gori et al. 2025); climatological mean shares	May misallocate losses for surge-dominated events; shifts allocation between the NFIP and wind insurers (ambiguous)
Insurance-system layers			
Private wind insurers (exposure)	Policy- or property-level premiums, coverage, and exposure by carrier and county	Statewide TIV (FHCF report) allocated across carriers by statewide market share (direct premiums written); uniform county shares	Tends to overstate the number of simultaneous defaults and FIGA assessments (upward bias)
Insurer capital	Full balance sheets, risk-based capital, internal models, parent guarantees, and cross-line support	Statutory surplus (entity and group) with a group-support rule	Omits support beyond the modeled group rule, overstating defaults (upward bias)
Reinsurance (FHCF)	Per-company FHCF elections and realized recoveries	Published FHCF reimbursement-contract terms and per-company elections (retention, coverage %, USD 17 B seasonal cap)	Closely matches actual terms (minimal bias)
Reinsurance (private treaties)	Per-carrier quota-share, excess-of-loss, retrocession, and industry-loss-warranty programs	Not represented (omitted)	Overstates net retained losses, hence defaults and FIGA assessments (upward bias)
Catastrophe bonds	Full insurance-linked-securities positions and triggers by sponsor	Public deal terms (Artemis); single-occurrence layers	May miss private placements, slightly overstating net losses (upward bias)
Insured share (wind)	Observed take-up and coverage adequacy by county and peril	Billion-Dollar Disaster reconstruction (≈40% in large events); Beta(4,6)	May overstate coverage: upward bias on insurer and FIGA stress, downward bias on modeled household burden (Table S6)
NFIP flood	Policy-level NFIP coverage and claims, plus the private-flood market	County coverage-in-force, take-up rates, Florida premium, and fund balance	Omits the small private-flood market; reasonable for the NFIP share (minimal bias)
Citizens	Policy-in-force and claims detail	Published county exposure, statutory surplus, Tier 1/Tier 2 premium bases	Good public coverage (minimal bias)
FIGA	Realized insolvency deficits and assessable-premium base	Statutory caps (2% normal plus 4% emergency) on surviving-insurer premium	Statutory caps applied as written (minimal bias)
NFIP backstop	Fund balance, reinsurance, and Treasury borrowing authority	Modeled fund pool (USD 3.441 B) plus Treasury borrowing	Omits the NFIP's reinsurance program, slightly overstating Treasury borrowing (upward bias)

Table S9: Model parameters and uncertainty treatment in the risk-propagation framework. Each parameter is classified as *deterministic* (held fixed across all simulations), *stochastic* (resampled each Monte Carlo iteration), or *uncertain* (varied across the climate-model ensemble). Data inputs and their public proxies are summarised separately in Table S8.

Parameter	Value	Source	Treatment
Stochastic (sampled each iteration)			
Insured wind fraction f_W	Beta$(4,6)$, mean 0.40	NOAA Billion-Dollar Weather and Climate Disasters reconstruction (Supp. Methods)	Stochastic; swept 0.1–0.5 (Table S6)
Wind/flood loss share	Beta prior, mean 0.846 (wind)	Gori et al. (2025), county P_{95}	Stochastic; drives flood-metric variance (Table S7)
TIV perturbation	CoV $= 0.15$	Assumed	Stochastic
Deterministic (fixed across simulations)			
Number of simulated seasons N	10,000	Model configuration	Deterministic
FHCF seasonal cap	\$17 B	FHCF statute / 2023–24 report	Deterministic
FHCF coverage election cov_i	$\{45, 75, 90\}\%$	FHCF reimbursement contract	Deterministic; assigned by insurer
FHCF retention and payout-limit multiples	retention multiples by coverage election: 12.15 (45%), 7.29 (75%), 6.07 (90%); payout-limit multiple 11.24; LAE multiplier 1.10	FHCF reimbursement contract	Deterministic
	FHCF reimbursement contract	Deterministic	
FIGA assessment cap	2% normal $+$ 4% emergency of surviving premium	Fla. Stat. §631.57	Deterministic
Citizens Tier 1 / Tier 2 caps	15% / 10% of respective premium bases	Citizens enabling statute	Deterministic
NFIP fund pool	\$3.441 B	CRS IN10784	Deterministic
Intragroup support rule	group/entity surplus ratio > 10; eligible deficits cured up to the available group pool	Stylized rule; surplus from S&P filings	Deterministic
Uncertain (varied across the climate ensemble)			
Climate-change deltas	5-GCM ensemble median, 10th–90th percentile range	CMIP6 / MIT TC model	Uncertain (ensemble range reported)